2023-04-10

Isolation of tumour-reactive lymphocytes from peripheral blood via microfluidic immunomagnetic cell sorting

Wang, Z

10.1038/s41551-023-01023-3
Nature Biomedical Engineering
Nature Research

Isolation of tumour-reactive lymphocytes from peripheral blood via microfluidic immunomagnetic cell sorting

Zongjie Wang[1,2], Sharif Ahmed[1], Mahmoud Labib[3], Hansen Wang[4], Licun Wu[2], Fatemeh Bavaghar-Zaeimi[2,5], Nastaran Shokri[5], Soraly Blanco[4], Saraf Karim[5], Kasia Czarnecka-Kujawa[5], Edward H. Sargent[6], AJ Robert McGray[7], Marc de Perrot[2,5,8], and Shana O. Kelley[1,3,4,9,10,11,12,13,*]

[1]Department of Biomedical Engineering, McCormick School of Engineering, Northwestern University, Evanston, IL, 60208, USA.
[2]Latner Thoracic Surgery Research Laboratories, Toronto General Hospital Research Institute, University Health Network, Toronto, M5G 1L7, Canada.
[3]Department of Chemistry, Weinberg College of Arts & Sciences, Northwestern University, Evanston, IL, 60208, USA.
[4]Department of Pharmaceutical Sciences, Leslie Dan Faculty of Pharmacy, University of Toronto, Toronto, M5S 3M2, Canada.
[5]Division of Thoracic Surgery, Toronto General Hospital, University Health Network, Toronto, M5G 2C4, Canada.
[6]The Edward S. Rogers Sr. Department of Electrical & Computer Engineering, University of Toronto, Toronto, M5S 3G4, Canada
[7]Department of Immunology, Division of Translational Immuno-Oncology, Roswell Park Comprehensive Cancer Center, Buffalo, NY, USA.
[8]Department of Immunology, Temerty Faculty of Medicine, University of Toronto, Toronto, M5S 1A8, Canada.
[9]International Institute for Nanotechnology, Northwestern University, Evanston, IL, 60208, USA.
[10]Department of Biochemistry, Feinberg School of Medicine, Northwestern University, Chicago, IL, 60611, USA.
[11]Robert H. Lurie Comprehensive Cancer Center, Northwestern University, Chicago, IL, 60611, USA.
[12]Simpson Querrey Institute, Northwestern University, Chicago, IL, 60611, USA.
[13]Chan Zuckerberg Biohub Chicago, Chicago, IL, 60611, USA.

*Corresponding author, shana.kelley@northwestern.edu

The clinical use of tumour-infiltrating lymphocytes for the treatment of solid tumours is hindered by the need to obtain large and fresh tumour fractions, which is often not feasible in patients with unresectable tumours or recurrent metastases. Here, we show that circulating tumour-reactive lymphocytes (cTRLs) can be isolated from peripheral blood at high yield and purity via microfluidic immunomagnetic cell sorting, allowing for comprehensive downstream analyses of these rare cells. We observed that CD103 is strongly expressed by the isolated cTRLs, and that in mice with subcutaneous tumours, tumour-infiltrating lymphocytes isolated from the tumours and rapidly expanded $CD8^+$ $CD103^+$ cTRLs isolated from blood are comparably potent and respond similarly to immune checkpoint blockade. We also show that $CD8^+$ $CD103^+$ cTRLs isolated from the peripheral blood of patients and co-cultured with tumour cells dissociated from their resected tumours resulted in the enrichment of interferon-γ-secreting cell populations with T-cell-receptor clonotypes substantially overlapping those of the patients' tumour-infiltrating lymphocytes. Therapeutically potent cTRLs isolated from peripheral blood may advance the clinical development of adoptive cell therapies.

The autologous transplantation of tumour-infiltrating lymphocytes (TILs) expanded from resected tumours has become a promising therapeutic modality in the clinic[1]. TIL-based adoptive cell therapy (ACT) has notable advantages over other allogenic and engineered cell therapies because of its inherent heterogeneity that maximizes the tumour-recognizing T cell receptors (TCRs) while minimizing off-tissue effects[2]. The clinical outcomes obtained with TILs to date are extremely encouraging – long-term complete responses have been observed in subsets of melanoma patients[3]. Despite the positive outcomes from pioneering clinical trials, the applicability of TIL-mediated ACT has primarily been demonstrated for metastatic melanoma, where resectable metastatic lesions are often large (> 3 cm in diameter), providing an optimal source material for TIL isolation[4]. However, for other solid tumours, such large lesions are not readily accessible. Moreover, in some cases excisional surgery may not be an option for patients due to a substantial risk or rapid tumour progression[5]. Recent studies have explored the possibility to apply TIL ACT to other solid tumours, such as renal carcinoma[6], cervical cancer[7], and breast cancer[8]. But limited functionality of TILs[6,8] and reduced response rates[7] were observed. Hence, new approaches that deliver active autologous cells are needed.

Advances in organoid development and deep sequencing have facilitated the generation of TIL-like tumour-reactive lymphocytes (TRLs) via the co-culture of peripheral blood lymphocytes with tumour-derived

organoids[9] or peptide pools from tumour-derived neoantigens[10]. However, these approaches still require a resection of primary tumour cells harvested using invasive surgical procedures. In addition, establishing organoids[9] and the synthesis of neoantigen-derived peptides[10] takes several weeks to complete. Overall, the requirement of tumour biopsy and lengthy workflow limits the translational value of these approaches as an alternative to TILs.

Prior work has confirmed the presence of TRLs in circulation at a very low frequency[11]. Given the intriguing possibility that tumour-reactive cells could be isolated non-invasively from blood, several studies have sought to characterize and isolate rare circulating TRLs (cTRL). Studies from multiple groups further substantiated the presence of cTRL in lung[12], and melanoma patients[13], even prior to immunotherapy[14]. However, personalized neoantigen-derived multimers were used to identify and isolate such a rare population from circulation[13–17], which requires the characterization of tumour neoantigens through invasive biopsy. In addition, a recent study on peripheral T cell dynamics after immunotherapy revealed that a subset of peripheral lymphocytes shares clonotypes with TILs, and that their expansion is highly correlated with response to treatment[18].

As multimer-based cTRL isolation may be difficult to translate into the clinic, the identification of more generalized markers for cTRLs is an important goal. Based on the surface markers that are known to influence the phenotypic properties of TILs, prior studies suggested that cTRLs may exhibit high expression levels for immune checkpoint markers such as PD-1[19] or CD39[20]. Yet, a more comprehensive analysis, ideally using an unbiased screening method, is needed to identify a biomarker that offers clear discrimination between cTRLs and their non-tumour reactive counterpart. The rarity of cTRLs remains a key challenge for the comprehensive analysis and therapeutic application of cTRLs, as most molecular approaches require at least several thousand cells as the input and millions of cells are required to test therapeutic efficacy. With levels as low as 0.002% in peripheral T cell populations[14], it is extremely difficult to enrich cTRLs with high purity and recovery for downstream analysis.

Here we describe a microfluidic approach that efficiently isolates cTRLs from blood circulation for rapid expansion and cellular therapy (Fig. 1a). Our approach is non-invasive and appears applicable to a variety of solid tumours on the basis of studies in mouse tumour models, and may therefore provide a practical alternative to existing TIL-mediate ACT. Our approach is built on immunomagnetic-cell-sorting technology[21] reported previously but now optimized for identifying and isolating cTRLs in PBMCs. With the high recovery and purity established, we identified CD103 as a molecular signature for cTRLs. Compared to immune checkpoint markers like PD-1 and CD39, CD103 is widely expressed by the tumour-reactive population in circulation. This population has a tissue-resident-like (T_{rm}-like) phenotype and has the capability to re-enter blood circulation from primary tumours and accumulate in secondary tumours. We subsequently show that the cTRLs can be expanded through a feeder-based rapid expansion protocol (REP) and that they have strong therapeutic potency in multiple adoptive-cell-transfer models in mice. We also confirmed that the enrichment based on $CD8^+CD103^+$ yields higher tumour reactivity in a small cohort of patient specimens by comparing the level of interferon gamma (IFN-γ) secretion and clonal similarity.

Results

Presence of cTRLs in circulation during tumour progression. We first sought to confirm the presence and fate of cTRLs in animal models. To confirm the presence of cTRLs, we pursued the isolation of cTRLs using this approach in animal models with two defined highly immunogenic epitopes - chicken ovalbumin ($OVA_{257-264}$, SIINFEKL) in C57BL6 models and influenza A hemagglutinin ($HA_{533-541}$, IYSTVASSL) in Balb/c models. Tumour cells with/without the expression of these defined epitopes were injected subcutaneously. Blood and tumour were collected at the mid-late stage (defined by 300 – 800 mm^3 tumour size) of tumour development and $CD8^+$ T cells were labelled by corresponding multimers and antibodies accordingly (Extended Data Fig. 1). Flow cytometric analysis indicated that mice bearing tumours expressing immunogenic epitopes exhibited a higher degree of immune response and slower growth of the tumours (Supplementary Fig. 1). The upregulated immune response produced a significantly higher fraction of TRLs specific to OVA/HA epitopes in tumour and blood (Extended Data Fig. 1 and Supplementary Fig. 2), which matches a previous observation for melanoma patients[14]. As expected, the percentage of TRLs is extremely low in blood (0.05% - 0.45% in $CD8^+$ T cells) – this highlights the intrinsic rarity of cTRLs.

Various recent reports suggest that the cTRLs have memory phenotypes,[18,22,23] which are believed to contribute to the adaptive immune response against similar pathogens, through homing to the infected sites for direct killing.[24] With this in mind, we established a tumour transplantation model to determine the destination of cTRLs in blood. In brief, an OVA-expressing tumour from the donor CD45.2 mice was transplanted as a whole to the host CD45.1 mice bearing a secondary (2^{nd}) tumour with/without OVA epitopes. Two tumours were allowed to grow simultaneously and the 2^{nd} tumours were collected at the end

for flow cytometric analysis (Supplementary Fig. 3). For all of the specimens analysed, we observed a small portion of CD45.2$^+$ cells presented in the 2nd tumour. Since the only source of CD45.2$^+$ T cells is the TILs within the transplanted tumour, this observation provides direct evidence that the TILs can enter the circulation and migrate to distant organs. In addition, we noticed that the 2nd tumours with OVA epitopes attract at least a 5-fold higher percentage of CD45.2$^+$ T cells compared to OVA-free WT tumours (Supplementary Fig. 3) – this suggests the migration and the accumulation of cTRLs are antigen-driven. Sites with similar patterns of infection (e.g. same immunogenic epitope) attract more cTRLs to re-infiltrate and reside. Taken together, the data collected indicates that the cTRLs commonly present in blood during tumour development, migrate towards and accumulate specifically in distal tumours (Fig. 1b).

High-performance cell isolation to enable cTRL profiling. The use of blood as source material and considerable levels of tumour specificity make cTRLs an ideal route to non-invasively acquire tumour-targeting lymphocytes for immunotherapy. However, there is a critical issue preventing the implementation of this idea, which is the use of major histocompatibility complex (MHC) multimers for cTRL identification during isolation. MHC multimers are derived from tumour neoantigens through invasive biopsy and off-the-shelf reagents are not available for individual patient samples. To develop a multimer-independent isolation workflow, it is important to comprehensively profile cTRLs and understand their unique clonal and molecular signatures (e.g. surface protein expression) that can serve as a specific biomarker for isolation.

Given that cTRLs are extremely rare (as low as 0.002%)[14] and difficult to analyse without purification, it is challenging to isolate rare cells efficiently with high levels of purity and recovery using conventional cell sorting techniques. For instance, fluorescence-activated cell sorting (FACS) cannot robustly discriminate rare cells when the target population is fewer than 0.2%[25,26]. Special protocols have been developed to increase the detection limits of flow cytometry to 0.001% by collecting a very large number of events (e.g. 1 x 10^9),[27,28] but this is not practical for real-world implementation. In addition, FACS typically loses 50 – 70% of target cells due to bad droplet formation or incorrect scanning[29,30]. The low performance of cell sorting may substantially impact the results of downstream molecular assays, such as TCR sequencing[21]. For example, our previous study has shown that FACS could only recover 684 clonotypes from isolated TILs while other purification approaches could recover up to 64,155 clonotypes simultaneously[21].

With this in mind, we hypothesized the introduction of a high-performance cell sorting technology would help to deconvolute the clonal and molecular profiles of cTRLs by effectively isolating these cells with high purity and recovery levels. The high-quality molecular profile of cTRLs would further contribute to the identification of multimer-independent biomarkers for cTRL isolation. We adapted a microfluidic system developed for sorting TILs from solid tumours based on surface markers[21] to the isolation of cTRLs from blood, firstly based on multimer binding for molecular profiling and later on based on identified surface markers that emerged from profiling studies. The system achieved up to 10-fold higher throughput and recovery compared to FACS while maintaining similar purity.

The overall workflow of the tumour reactivity-mediated cell labelling and sorting strategy is illustrated in Figure 2a. Lymphocytes are treated with MHC multimers mimicking a defined tumour epitope to selectively isolate a subset of TRLs with putative tumour reactivity. The multimers are conjugated with a fluorophore, which is used as a linker to attach magnetic nanoparticles (MNPs). To separate the multimer-binding lymphocytes, or tumour-reactive lymphocytes, magnetically labelled cell mixtures are processed with a microfluidic device sandwiched by arrays of magnets (Supplementary Fig. 4). The device contains multiple capture zones that can spatially separate cells with different degrees of magnetization – a higher degree of magnetization results in the capture in a compartment close to the inlet (Supplementary Fig. 5)[31,32]. In the case of multimer-mediated labelling, the TRLs are captured here while the non-TRL populations are captured in a different compartment. Captured cells can be easily and efficiently recovered from the device compartments when the external magnets are removed. Recovered cells are highly viable and suitable for downstream culture and analysis[25,26]. Details of the working principle of the device can be found in the supporting discussion (SD). As previously reported[21], the microfluidic cell sorting outperforms commercial cell sorting techniques when recovering rare cell populations. For multimer-mediated labelling and sorting, it is worth noting that the purity of FACS post-isolation is better than microfluidics (89% vs 75%, Extended Data Fig. 2), which may be beneficial to purity-focused applications such as TCR derivation. However, our microfluidic approach achieved up to 10-fold higher cell recovery compared to FACS and therefore is more suitable for molecular assay and cellular therapies. We pursued the isolation of cTRLs using this approach in the defined epitopes model described above. We utilized a workflow consisting of negative capture of CD8$^+$ lymphocytes, followed by positive selection multimers through immunomagnetic cell sorting (Fig. 2b). The purity of isolation is 76% for OVA (Extended Data Fig. 2) and 84% for HA multimers (Fig. 2c), respectively.

The high yield and purity from microfluidic sorting enabled us to perform direct TCR sequencing on the rare cTRL populations (Fig. 2d). We identified over 1,000 clonotypes (defined by the unique CDR3 sequence) in

the cTRLs from 10 – 15 mL pooled mouse whole blood. Mapping of V-J usage reveals a high level of similarity between cTRLs and intratumoural TILs, rather than the non-reactive portion of peripheral blood mononuclear cells (PBMCs). In terms of the TCR repertoire, cTRLs cover 30% - 85% of the top 50 clones presented in TILs, 3 – 8 times higher than the coverage observed in non-cTRL PBMC (~10%, Fig. 2e). We also analysed the percentage of top-20 TIL clones by fraction in cTRLs and non-cTRL $CD8^+$ PBMC and observed a notable enrichment of TIL clones in cTRLs (Tab. 1). Taken together, these data suggest that the cTRLs exist in the circulation during disease progression and share a higher degree of clonal similarity with intratumoural TILs.

The high yield and purity from microfluidic sorting also allowed RNA sequencing (RNAseq) to be performed on the rare cTRL population. For the OVA-reactive cTRLs isolated from the melanoma model, a tissue-resident memory (T_{rm}) phenotype was detected with strongly upregulated expression of *ITGAE* compared to non-cTRL bulk $CD8^+$ cells (Fig. 3a, left) and upregulated expression of *ZFP683*, a transcriptional hallmark of T_{rm} (Fig. 3a, right). In addition, cTRLs expressed a higher level of exhaustion, cytotoxicity, and activation markers compared to other dedicated T cell subpopulations in PBMC, including naïve T cells ($T_{naïve}$, $CD8^+CD45RA^+$) and memory T cells (T_{mem}, $CD8^+CD45RA^-$). This further revealed that cTRLs have a partially exhausted yet activated tissue-resident memory phenotype. Gene set enrichment analysis (GSEA) also suggests that the cTRLs have statistically significant upregulation of T cell activation and TCR signaling pathways (Supplementary Fig. 6). We observed a similar trend of marker expression in HA-reactive cTRLs isolated from the colon cancer model (Supplementary Fig. 8). By overlaying the differentially expressed genes, we identified 12 shared upregulated genes. Genes that are known to be transiently or permanently upregulated during TCR-MHC interaction (e.g. *GGT1*[33], and *CD8A*[34]) were eliminated from this subset. One of the strongest hits observed was *ITGAE*, a gene that encodes CD103. In fact, the expression of CD103 on healthy PBMCs is relatively low at the protein level, according to a comprehensive mass cytometry study[35]. This further suggests the utility of CD103 as a specific marker for cTRL isolation.

To further evaluate this finding, circulating $CD8^+$ lymphocytes were isolated from mice bearing B16F10 and AE17 cancer cell lines expressing the OVA epitope. Flow cytometric analysis indicated that CD103 is widely expressed by the OVA-reactive cTRLs (Fig. 3b). Collectively, about 30% of the $CD8^+CD103^+$ cells in circulation are OVA-reactive (Fig. 3c), which yields up to 50-fold enrichment of OVA-reactive T cells. It is perhaps not surprising that $CD103^+$ helps to define tumour-reactive populations in bulk T cells as previous studies have suggested CD103, alone[36,37] or together with other markers[38], defines T cells with elevated potency for adoptive cell therapy and immune checkpoint blockade. However, it is interesting that such T_{rm}-like phenotype, which is believed to reside in non-lymphoid tissue[39], is present in circulation. Therefore, we further confirmed the signature of migrating and migrated cTRLs in the aforementioned tumour transplantation model (Supplementary Fig. 3) by cytometry by time of flight (CyTOF). During migration, over 80% of the cTRLs (defined as the multimer-binding $CD3^+CD8^+$ T cells) were $CD103^+$ (Fig. 3d and 3e). And CD103+ cTRLs consist of a large portion of PD-1^+, $CD39^+$ or $CD69^+$ cells (Supplementary Fig. 9). Post migration, compared to the $CD45.1^+$ endogenous T cells, $CD45.2^+$ cTRLs still had higher expression of $CD103^+$, $CD69^+$, and PD-1^+ (Fig. 3f and 3g), suggesting they retained the T_{rm}-like, activated phenotypes after migration. Indeed, this observation is consistent with the emerging evidence showing T_{rm} enter circulation to increase the overall immune response[40,41]. Mechanistically, CD103 is an integrin protein that binds to E-cadherin and governs the formation of cell protrusions/filopodia[42], an essential component for initiating cell migration[43]. This points to the critical role of CD103 in cell motility and moreover, $CD103^+$ TRLs are reported to have elevated energetic potential and greater migration capacity[44]. Hence, the phenotypic properties of cTRLs are consistent with prior observations of $CD103^+$ T cells.

Expansion and administration of cTRLs for ACT. The use of high-performance microfluidics together with the newly identified biomarker CD103 provides a simple approach to isolate cTRLs from PBMC for adoptive cell therapy. We firstly optimized the microfluidic cell sorting based on CD103 and achieved up to 16-fold higher cell recovery (73.3% vs 4.5%) compared to FACS while retaining similar purity (Extended Data Fig. 3). Subsequently, we adapted the rapid expansion protocol (REP) of rare tumour-reactive TILs[45] and achieved up to 2000-fold expansion of cTRLs in 10 days (Supplementary Fig. 10 and 11), yielding the final number of cTRLs around 0.1 – 4 million per mouse. We did not compare the yield of FACS-sorted samples since its low recovery did not grant robust cell growth during REP. The cTRLs maintained their T_{rm}-like phenotypes upon expansion (Supplementary Fig. 12), including a high expression of critical surface (CD103 and CD69) and intracellular cytotoxic markers (IFNG and GZMB). It is also worth noting that about 70% of the cTRLs are PD-1^{med}TIM3$^-$, indicating a partially exhausted yet tumour-reactive phenotype[46,47]. An *in vitro* killing assay revealed that expanded cTRLs lysed 65% of the cells in 24 hrs (Supplementary Fig. 13). Such killing potency is comparable to TILs. We also elaborated a continuous antigen exposure model[48] to assess the degree of exhaustion (Supplementary Fig. 13). Compared to TILs subjected to REP, expanded cTRLs showed greater killing potency over 3 rounds of antigen exposure, suggesting a strong anti-exhaustion

phenotype. This result is in line with a recent pan-cancer analysis suggesting that the $CD8^+ZNF683^+$ T_{rm} subpopulations have a lower frequency of terminally exhausted T cells[49].

We next characterized the therapeutic efficacy of cTRLs *in vivo* using multiple animal models. We first benchmarked the therapeutic potency of expanded TILs, cTRLs, and $CD8^+CD103^-$ PBMC populations with subcutaneous B16F10 melanoma (Fig. 4a – 4b, Supplementary Fig. 14 and 15) and LLC1 NSCLC model (Extended Data Fig. 4). We confirmed that cTRLs have improved therapeutic potency compared to $CD8^+CD103^-$ PBMCs. It is worth noting that we expanded the $CD8^+CD103^-$ PBMCs using a feeder-free protocol due to their abundance. The feeder-free protocol may cause more severe activation-induced cell death (AICD) and/or fratricide compared to feeder-based protocol[50]. However, it is unlikely that the selective expansion of $CD8^+CD103^-$ PBMCs will impact their anti-tumour potency given their low tumour reactivity post-isolation (Fig. 3b and 3c).

The potency of cTRLs is comparable to the TILs isolated from solid tumours – both extending median survival by 40% - 50%. This suggests that the TCR repertoire of the cTRLs, although not as diverse as the TILs, exhibits sufficient tumour-reactive TCRs for tumour killing. In addition, we verified the feasibility of treating metastases with cTRLs using an induced metastasis model by tail-vein injection of 4T1 cells (Fig. 4c – 4d) – the group treated by cTRLs had a 30% increase in the median survival and a 60% reduction in the lung metastases (Extended Data Fig. 5) compared to the $CD8^+CD103^-$ PBMC group. It is worth noting that no primary tumour was involved during the cTRL isolation and reintroduction – this suggests that the use of cTRLs is applicable to a broader group of patients, including individuals with unresectable tumours or who underwent surgery (without TIL isolation/expansion) and went to developed recurrent metastasis. Taken together, our findings indicate that the cTRLs have notable therapeutic potency and could be used in conjunction with a more practical harvesting process. However, we observed that monotherapy using cTRLs was insufficient for long-term tumour management, with less than 20% of the mice in this study experienced a complete response (CR) at study endpoint.

To further improve the therapeutic efficacy of cTRLs, we next tested the combination of cTRLs with immune checkpoint blockade (ICB). We hypothesized that the cTRLs would respond to the ICB considering their $PD\text{-}1^{med}TIM3^-$ partially exhausted phenotype. In addition, existing studies showed that the percentage of $CD8^+CD103^+$ T_{rm} predicts response to ICB therapy – further supporting this rationale[36,37]. To test this hypothesis, we elaborated a MC38 colon cancer model in immunocompromised mice ($RAG^{-/-}$) and treated them with the combination of cTRLs and anti-PD-1 blockade (Extended Data Fig. 6), to solely test the effects of ICB on infused cTRLs. As anti-PD-1 blockade requires the T cells to function, we observed little difference between the untreated and anti-PD-1 groups in $RAG^{-/-}$ backgrounds that resulted in no mature T cells. Monotherapy of cTRLs produced transient tumour control for about 2 weeks but underwent rapid tumour progression after this time point. A cocktail of anti-PD-1 and cTRLs was observed to exhibit durable tumour control over 4 weeks and extended the median survival by 100% compared to the untreated group. IHC analysis comparing the resected tumours from the cTRLs and the cocktail revealed a large difference in the number of infiltrated $CD8^+$ T cells (1.2% vs 3.2%). Taken together, this immunocompromised model provides direct evidence that the cTRLs are responsive to ICB and the cocktail of cTRLs and ICB can achieve long-lasting tumour control.

In addition to direct tumour killing, T_{rm} is also known to utilize other mechanisms for tumour control, such as the new recruitment of other immune cells[51]. To gain insights related to these indirect processes, we used a MC38 model in immunocompetent mice ($CD45.1^+$) and treated them with the $CD45.2^+$ cTRLs and ICB (Fig. 5a). With intact endogenous immunity, the cocktail of cTRLs and ICB achieved remarkable tumour control, with 5 out of 5 mice surviving at study endpoint and 4 mice exhibiting complete response (CR). To better understand how cTRLs and ICB altered the tumour microenvironment (TME), pathway enrichment was performed on the upregulated genes from gene expression analysis (Fig. 5b). Although both treatments upregulated the overall adaptive immune response, we noticed that the type of enriched immune pathways was different between the treatments, with PD-1 ICB significantly altering the PD-1/L1 pathways and enhancing the immune effector functions, while cTRLs promoted migration and activation of other immune cells, including granulocytes, B cells, and NK cells. The cocktail of PD-1 ICB and cTRLs further boosted the differentiation of helper T cells and phagocytosis. IHC analysis on CD4 and CD208 (DC-LAMP) further confirmed this observation at the protein level (Fig. 5c). Taken together, these data indicate that cTRLs prompt additional immune cells to infiltrate while ICB can improve the functionality of infiltrated immune cells – hence co-administration of cTRLs and ICB shows synergistic effects. In addition, it is worth noting that the antitumour immunity against the MC38 tumour is durable as observed through tumour rechallenge experiments conducted 3 months post initial therapy (Fig. 5d). Flow cytometric analysis using a MC38 derived multimer (SIIVFNLL) confirmed the presence of tumour-reactive memory T cells of both $CD45.1^+$ and $CD45.2^+$ origin, providing direct evidence that the cTRLs participate in the establishment of long-term anti-tumour immunity.

In addition to ICB, we also confirmed that the cocktail of cTRLs and co-stimulatory molecules (e.g. GITR) can yield synergistic effects when treating mouse mesothelioma (Fig. 5e). The combination of anti-GITR antibodies and cTRLs yields 47% extended median survival compared to untreated animals. CyTOF analysis revealed that the administration of cTRLs promoted the infiltration of endogenous CD4 and CD8 cells (Fig. 5f and Supplementary Fig. 16), similar to what we have observed in the MC38 model. The cocktail of cTRLs and anti-GITR antibodies upregulated the frequency of $CD8^+$ and $CD8^+PD\text{-}1^+$ cytotoxic T cells and reduced the number of $CD4^+CD25^+$ regulatory T cells (Supplementary Fig. 16), generating a more proinflammatory TME for better tumour control. This observation matches with the intrinsic function of T_{rm} cells – that is to secrete proinflammatory cytokines at the diseased site to trigger downstream adaptive immune response[52]. We also investigated the phenotype of intratumoural cTRLs at endpoint (Fig. 5g). Compared to endogenous $CD8^+CD45.1^+$ cells, $CD45.2^+$ cTRLs still maintained high expression of CD103. Taken together, we conclude that the T_{rm}-like phenotype permits the expanded cTRLs a strong ability to not only perform direct killing on tumour cells, but also to bolster the endogenous intratumoural adaptive immune response.

Isolation and validation of human cTRLs. To investigate the presence of cTRLs in human specimens, we acquired paired malignant pleural effusion (MPE) samples and PBMCs from 6 immunotherapy-naïve patients' samples. We co-cultured the bulk PBMCs with $CD45^+$ depleted MPE-derived tumour cells and measured the fraction of IFN-γ secreting cells in $CD8^+CD103^-$ and $CD8^+CD103^+$ subpopulations by intracellular flow cytometry post 12 - 24 hours (Fig. 6a). The panel for flow cytometry included CD103 FMO (fluorescence minus one) and unstimulated (PBMC alone) controls for the precise identification of $CD103^+$ populations (Fig. 6b). We observed a small portion of interferon gamma (IFNγ) secreting cells in the unstimulated control (5.3% for $CD103^+$, 7.4% for $CD103^-$). When stimulated by MPE-derived tumour cells, a notable portion of $CD103^+$ T cells exhibited IFNγ secretion (51%) while the percentage of IFNγ secreting $CD103^-$ T cells remained roughly unchanged (8.4%). This observation suggested that the IFNγ secretion in $CD103^+$ T cells is tumour-dependent. Hence, the expression of CD103 may also define cTRL population in human specimens (Fig. 6c).

To gain more insight on the tumour reactivity of human $CD8^+CD103^+$ cTRLs, we acquired a small cohort of patients with a variety of solid tumour (N = 20). The major tumour types in this study included colon, mesothelioma, lung and breast (Fig. 7a). We isolated $CD8^+CD103^+$ cTRLs from PBMCs and co-cultured them with dissociated tumour cells (DTCs) or MPE-derived cancer cells and assessed their tumour reactivity by IFNγ secretion (Fig. 7b – 7c). Compared to the bulk $CD8^+$ T cells, we consistently observed a global increase of IFN-γ secretion after CD103-mediated isolation, suggesting that sorting based on $CD8^+CD103^+$ helped to define and enrich for a tumour-reactive T cell subpopulation. We found the presence of cTRLs is common in immunotherapy-naïve PBMC – this is in line with the previous study reporting neoantigen-reactive T cells can be detected prior to immunotherapy[14]. In addition, we assessed the tumour reactivity of the isolated $CD8^+CD103^+$ cTRLs across the DTCs from different patients (Supplementary Fig. 17). We found that IFNγ secretion of cTRLs was patient-specific – the isolated cTRLs experienced the highest IFNγ secretion on autologous tumour cells. This highlights the patient-specific tumour reactivity of cTRLs at the phenotypic level.

In a subset of patients, we also isolated the TILs, cTRLs, and $CD8^+CD103^-$ PBMC for TCRseq using a workflow similar to Fig. 1B. Among three sequenced samples, we consistently observed similarity between the major clones presented in TILs and cTRLs (Fig. 7d – 7e). For example, in the case of CA03, cTRLs share 4 major clones with TILs – TRAV2/TRAJ37, TRAV25/TRAJ37, TRAV20/TRAJ53, and TRAV5/TRAJ18 (Fig. 7D). Over 25% of the cTRLs belong to one of these four clonotypes. In contrast, only 0.6% of the $CD8^+CD103^-$ PBMC fall into these clonotypes. Overall, similar to mouse samples, $CD8^+CD103^+$ cTRLs cover about 35 - 60% of the top 50 clones (ranked by fractions) presented in $CD8^+$ TILs (Fig. 7e). The significant overlap of TCR proves the tumour reactivity of $CD8^+CD103^+$ cTRLs from the perspective of clonal analysis. This is in line with a set of prior studies reporting that the positive expression of CD103 defines the tumour-reactive TILs across human breast[53], lung[54], cervical[55], and oral cancer[56].

Bioinformatic analyses also predicted their strong therapeutic potential of human $CD8^+CD103^+$ cTRLs. For example, the TIMER (Tumour IMmune Estimaition Resource) algorithm[57] reveals that the expression of CD103 has strong correlation with a high level of immune infiltration in many cancer types (Supplementary Fig. 18) using predicted immune cell fraction from bulk RNAseq[58]. In addition, the TIDE (Tumour Immune Dysfunction and Exclusion) algorithm[59] on the mRNA-seq data across 194 cohorts of solid tumours shows that the upregulated expression of intratumoural *ITGAE* correlates with statistically lower death risk and good prognosis over multiple cancer types (Supplementary Fig. 19). Furthermore, a meta-analysis involving 2,824 patients reports that patients with intratumoural $CD103^+$ immune cells were associated with favorable survivals[60]. Taken together, our clonal and phenotypic analyses showcased that the expression of CD103 defines the cTRL population in human PBMC.

Outlook

Thus far, the production of therapeutic TILs has required an accessible tumour lesion for excisional biopsy as source material for TIL isolation and expansion. However, such lesions are not always available from patients and, moreover, surgery on patients bearing unresectable cancers can pose a substantial risk[5]. The discovery of cTRLs in blood circulation highlights a new strategy for isolating therapeutic cells for ACT. The minimal invasiveness of blood collection makes the cTRL acquisition a more feasible and amenable process for the patients compared to TIL therapy. In addition, our analyses reveal that the cTRLs have sufficient coverage of dominant clones in TILs and are primed to target similar tumour microenvironment. These unique characteristics grant their therapeutic potency against metastatic tumours. Hence, the implementation of cTRLs would greatly extend the applicability of adoptive cell therapy and may provide a new treatment option for late-stage patients with unresectable and/or metastasized tumours.

Another outstanding issue for TIL therapy is the low CR rates (< 20%) in non-melanoma cancer in the clinic. At present, it is unclear which phenotypes of TILs should be used and how often should TILs be administrated to deliver a persistent therapeutic outcome[61]. We noticed that the cTRLs were responsive to immune checkpoint blockade (ICB) and co-stimulatory molecules – the combination of ACT and ICB achieved 80% CR rate in mouse colon cancer models. Considering the ease of collection/administration of cTRLs, the cocktail of ACT and ICB may hold promise as an immune-oncology combination. In addition, although the enrichment based on CD103 results in relatively pure $CD8^+$ cTRL populations, the best marker combinations for cTRL isolation may require a more comprehensive comparison. Also, it remains to be explored if the dose of 'pure' cTRLs is sufficient to achieve durable responses in patients. Indeed, recent studies suggest that a more diverse and memory-like cell population may perform better on a long-term basis[62]. Therefore, it may be necessary to pool cTRLs with other T cell subpopulations to deliver durable therapeutic outcomes.

Taken together, our study provides new evidence supporting the presence of $CD8^+$ tumour-reactive lymphocytes in circulation and highlights the usefulness of such a population for cancer immunotherapy. Future studies shall focus on verifying the therapeutic potency of cTRLs in humanized models. In addition, a recent study revealed the presence of $CD4^+$ tumour-reactive lymphocytes in circulation[63]. Biomarkers for $CD4^+$ cTRLs is an additional area of importance considering the critical roles of $CD4^+$ T cells in the long-term success of ACT[64].

Methods

Cell culture. B16F10 mouse melanoma cells (RRID: CVCL_0159), CT26 mouse colon cancer cells (RRID: CVCL_7254), and LLC1 mouse lung cancer celle (RRID: CVCL_4358) were purchased from ATCC (Manassas, VA) and cultured in Roswell Park Memorial Institute 1640 (RPMI-1640) medium supplied with 10% fetal bovine serum (FBS, Wisent). AE17 mouse mesothelioma (RRID: CVCL_4408) were purchased from ECACC (Porton Down, England) and maintained in RPMI-1640 with 10% FBS. MC38 mouse colon cancer cells (RRID: CVCL_0A68) and KPCY 6419c5 mouse pancreatic cancer cells (RRID: CVCL_YM21) were purchased from Kerafast (Boston, MA) and cultured in Dulbecco's Modified Eagle Medium (DMEM, high-glucose) with 10% FBS. $B16F10^{OVA}$, and $AE17^{OVA}$ cells were established by lipofection using lipofectamine 3000 (Thermo) and SIINFEKL-GFP-puro plasmid (#102944, Addgene, Watertown, MA), followed by two rounds of 5-day puromycin selection. $CT26^{HA}$ cells were established as described previously.[65] 4T1-Luc2 mouse breast cancer (RRID: CVCL_A4BM) were purchased from ATCC and maintained in RPMI-1640 with 10% FBS and 8 μg/mL blasticidin (BLA477.100, BioShop, Canada).

Mouse models for cTRL analysis and isolation. All animal experiments were carried out in accordance with the protocol approved by the Animal Care Committee of Northwestern University and/or University Health Network. Female C57/BL6J strains of mice at 6 to 8 weeks of age were purchased from the Jackson Laboratory (Bar Harbor, ME). Female Balb/c strains of mice at 6 to 8 weeks of age were purchased from Jackson Laboratory. All mice are maintained at the animal facility under a 12/12 dark cycle.

For $B16F10^{OVA}$ models, 5×10^5 $B16F10^{OVA}$ or B16F10 cells were engrafted subcutaneously (s.c.) on the right flank of C57BL6J mice. On day 14, mice were euthanized for blood, spleen, and tumour isolation. For $CT26^{HA}$ models, 5×10^6 $CT26^{HA}$ or CT26 cells were engrafted s.c. on the right flank of Balb/c mice. On day 18, mice were euthanized for blood, spleen and tumour isolation. For $AE17^{OVA}$ models, 3×10^6 cells were engrafted s.c. on the right flank of C57BL6J mice. On day 16, mice were euthanized for blood and tumour isolation. For MC38 models, 5×10^6 cells were engrafted s.c. on the right flank of C57BL6J mice. On day 21, mice were euthanized for blood and tumour isolation. For KPCY 6419c5 models, 2×10^6 cells were engrafted s.c. on the right flank of C57BL6J mice. On day 21, mice were euthanized for blood and tumour isolation. For

4T1-Luc2 models, 2 x 10^5 4T1-Luc2 cells were injected intravenously (i.v.) to Balb/cJ mice. On day 21, mice were euthanized for blood isolation.

The mouse blood was collected through cardiac puncture. The blood was lysed in 1X RBC lysis buffer (00-4333-57, Thermo) for 5 min at RT and used for downstream flow cytometric analysis or magnetic isolation. The spleens were mechanically dissociated by cell scrapers through 70 μm cell strainers. Dissociated splenocytes were lysed by 1X RBC lysis buffer for 3 mins at room temperature (RT) and used for downstream flow cytometric analysis or magnetic isolation. The tumours were sectioned into 2 – 4 mm^2 pieces and dissciated with the mouse tumour dissociation kit (150-096-730, Miltenyi) using the gentleMACS C tubes (130-093-237, Miltenyi Biotec, Germany) and gentleMACS Dissociator (130-093-235, Miltenyi), according to manufacturer's protocol. Cell mixture was filtered twice by 70 μm strainers prior to downstream flow cytometric analysis or magnetic isolation.

For flow cytometric analysis, cells were stained by fluorescently labelled multimers at 2 – 8 ^oC for 30 min, followed by the staining of CD8α-APC at RT for 20 min in 1X phosphate-buffered saline (PBS) with 1% bovine serum albumin (BSA, A9418, Sigma). Stained samples were analysed by an acoustic flow cytometer (Attune NxT, Thermo) with a 2-laser 7-colour setup. Due to the rarity of tumour-specific T cells, at least 500,000 events were recorded for each sample. Acquired data were analysed by FlowJo software (FlowJo LLC., Ashland, OR).

For magnetic isolation, cells were stained by untouched mouse CD8 cells kit (11417D, Thermo) and sorted by the MATIC chips at the flow rate of 16 mL/hr. Negative portions were collected and stained by fluorescently labelled multimers targeting OVA or HA at 2 – 8 ^oC for 30 min, followed by anti-fluorophore magnetic particles with 50 nm diameter (Miltenyi) at RT for 20 min in 1X PBS with 1% BSA. Labelled cell samples were sorted by the MATIC chips using the flow rate of 4 mL/hr to capture tumour-reactive T cell population. For CD103-mediated sorting, negative portions collected from the first run were stained by anti-CD103 APC at RT for 20 mins in 1X PBS with 1% BSA, followed by anti-APC magnetic particles (130-090-855, Miltenyi) at RT for 20 mins in 1X PBS with 1% BSA. Labelled cell samples were sorted by the MATIC chips using the flow rate of 10 mL/hr to capture $CD103^+$ cells. Details of chip setup was describe in the section of 'chip fabrication and operation'.

Chip fabrication and operation. The MATIC microfluidic cell sorter was fabricated using the protocol described before.[21] In brief, the master mold was 3D printed by a stereolithographic 3D printer (Microfluidics Edition 3D Printer, Creative CADworks, Canada) using the "CCW master mold for PDMS" resin (Resinworks 3D, Canada) with the layer thickness of 25 μm. The chips were made by casting PDMS (Sylgard 184, Dow Chemical, Midland, MI) on printed molds, followed by 30-min incubation at 100 ^oC. Cured PDMS replicas were peeled off, punched and plasma bonded to thickness no. 1 glass coverslips (260462, Ted Pella, Redding, CA) to finish the chip. Prior to use, the chips were conditioned by 1X PBS with 1% sterlie Pluronic F68 (24040032, Thermo) to reduce non-specific cell capture. During experiments, each chip was sandwiched by arrayed N52 NdFeB magnets (D14-N52, K&J Magnetics, Pipersville, PA) and connected to a digital syringe pump (Fusion 100, Chemyx, Stafford, TX) for fluidic processing.

To form the sorting setup for mouse samples, the modules with 200 μm thickness were chosen to form a binary setup, which is able to separate cells into 2 populations (on-chip, effluent) based on its degree of magnetic labelling. For the isolation of cTRLs, the flow rate was optimized to 16 mL/hr and 4 mL/hr for the first (CD8 negative selection) and second run (multimer positive selection) by a preliminary run using RBC-lysed blood samples. For the CD103-mediated second runs, the flow rate was set to 10 mL/hr. For the isolation of TILs, the flow rate was set to 16 mL/hr, as optimized before.[21] For the CD45RA-mediated isolation of naïve and memory T cells, the flow rate was set to 32 mL/hr, as optimized before.[21]

To form the sorting setup for human samples, the modules with 200 μm thickness were chosen to form a binary setup. For the isolation of cTRLs, the flow rate was set to 24 mL/hr and 12 mL/hr for the first (CD8 negative selection) and second runs (CD103 positive selection). For the isolation of TILs, the flow rate was set to 24 mL/hr.

Comparison of isolation efficiency. The comparison of isolation efficiency among FACS, MACS, and MATIC is carried out by spiked-in blood samples. OT-1 $CD8^+$ mouse cytotoxic T cells were isolated from the spleen of OT-1 mice (C57BL/6-Tg(TcraTcrb)1100Mjb/J, 003831, Jackson) using a magnetic separation kit (130-096-543, Miltenyi Biotec). Isolated T cells were activated and expanded with CD3/CD28 beads (130-093-627, Miltenyi or 11452D, Thermo) at the cell/bead ratio of 1:1 for the first 3 days in Iscove's Modified Dulbecco's Medium (IMDM) and cultured up to 6 days supplied with 10% FBS and 100 ng/mL mouse interleukin 2 (130-120-662, Miltenyi) prior to the spike-in experiment. The spike-in sample is generated by spiking 0.5% of OT-1 cells into the RBC lysed blood from tumour-free C57BL6 mice. Spike-in samples were

stained by PE labelled multimers targeting OVA at 2 – 8 ^{o}C for 30 min, followed by anti-PE magnetic particles with 50 nm diameter (Miltenyi) at RT for 20 min in 1X PBS with 1% BSA (for MACS and MATIC and only). Labelled cell samples were sorted by the FACS based on the intensity of PE channel and MACS or MATIC based on the degree of magnetic labelling. FACS was performed by a BD FACS Aria IIIu by gating FSC/SSC and PE channels. MACS was performed by MACS LS columns (130-042-401, Miltenyi) using the QuadroMACS separator (130-091-051, Miltenyi). MATIC was performed using the condition described in the section of 'chip fabrication and operation'. Purity of unsorted and sorted samples was assessed by an acoustic flow cytometer (Attune NxT). Recovery of sorted samples was calculated based on the number of recorded PE^{+} cells, normalized to the unsorted sample.

TCR sequencing. Isolated mouse CD8^{+} T cell populations were centrifuged to from cell pellets and submitted to MedGenome (Foster City, CA) for bulk TCR sequencing using a SMARTer mouse TCR a/b profiling workflow (634402, TakaraBio, Japan). Isolated human CD8+ T cell populations were centrifuged to form cell pellets and submitted to MedGenome for bulk TCR sequencing using a SMARTer human TCR a/b profiling workflow (635016, TakaraBio). After library preparation, sequencing is performed using the 600 cycle kit on an Illumina MiSeq platform (San Diego, CA). Data generated is demultiplexed and trimmed. MiXCR (version 2.1.11) software was used to align the reads to the TCR clonotypes and assemble the final CD3 and full-length clonotypes. VJ gene usage was also extracted from the MiXCR data, including VJ gene usage.

RNA sequencing. Isolated CD8^{+} T cell populations were centrifuged to from cell pellets and submitted to MedGenome (Foster City, CA) for bulk mRNA sequencing using a SMART-seq v4 workflow in an ultra-low input fashion (634888, TakaraBio, Japan). Prepared libraries were sequenced by an Illumina HiSeq platform. Alignment was performed using STAR (v2.7.3a) aligner. Reads mapping to ribosomal and mitochondrial genome were removed before performing alignment. The raw read counts were estimated using HTSeq (v0.11.2). Read counts were normalized using DESeq2 to get the normalized counts. Additionally, the aligned reads were used for estimating expression of the genes using cufflinks (v2.2.1). Differential gene expression was calculated based on normalized counts.

Cytometry by time of flight (CyTOF). Single-cell suspension from TIL migration model were cyropreserved immediately without culture and activation. Cells were thawed and submitted to the centre for advanced single cell analysis (CASCA) at the SickKids Research Institute for cytometry by time of flight (CyTOF). Cells were stained using the protocol recommended by Fluidigm (San Francisco, California) and examined by a Helios CyTOF system. The antibodies used in CyTOF were listed in Supplementary Table 3. Acquired data were processed by FlowJo v10.5 (FlowJo LLC, Ashland, OR) by gating center, width, residual, and 193Lr-DNA2 channel. Built-in tSNE and plugins (FlowSOM and Cluster Explorer) were used for high-dimensional analysis.

Expansion of cTRLs. For standard TILs isolated from the tumour, the TILs were cultured on 24-well or 12-well plates for 3 days at the density of 0.5 - 1 x 10^{6} cells/mL in IMDM supplied with 10% FBS, 2X GlutaMAX (35050061, Thermo), 500 ng/mL mouse interleukin 2. TILs were activated with CD3/CD28 beads at the cell/bead ratio of 1:1 for the first 3 days. TILs were subcultured every 2 – 3 days to maintain the cell density of 1 x 10^{6} cells/mL.

For cTRLs isolated from the blood, the TILs were co-cultured with the feeder CD45.1^{+} CD8^{+} T cells isolated from the spleen, at the donor:feeder ratio of 1:50 – 1:100 in IMDM with 10% FBS, 2X GlutaMAX, 500 ng/mL mouse interleukin 2, 25 - 50 ng/mL mouse interleukin 15 (566302, Biolegend, San Diego, CA) and 10 - 20 ng/mL recombinant mouse TGF-beta (763104, Biolegend). The feeder cells were isolated from spleen as described above, expanded with CD3/CD28 beads in IMDM with 100 ng/mL mouse interleukin 2 for 3 days and received 30 – 35 Gy irradition through a Cs-137 source to inhibit proliferation prior to co-culture. During co-culture, cTRLs were activated with CD3/CD28 beads (130-093-627, Miltenyi or 11452D, Thermo) for the first 3 days and received medium renewal at day 3, 5 and 7. Post day 7, cTRLs were subcultured every 2 – 3 days to maintain the cell density of 1 x 10^{6} cells/mL.

Fold of expansion was calculated based on the ratio of CD45.2/CD45.1 staining through flow cytometry. All cultured TILs were cyropreserved at day 10 – 14 with a freezing medium containing 90% FBS 10% DMSO. TILs were thawed 1-2 days prior to downstream *in vitro* assays and *in vivo* transplantation.

Adoptive transplantation. For B16F10 models, female C57/BL6J strains of mice at 6 to 8 weeks of age were s.c. engrafted with 5 x 10^{5} B16F10^{OVA} on the right flank of mice. On day 7, 1 x 10^{6} TILs, CD8^{+}CD103^{-} PBMC, or cTRLs (CD8^{+}CD103^{+}) were injected intraverscularly (i.v.). All mice received the injection of 10 µg IL-2 injection on day 8, 9 and 10. For LLC1 models, femable C57/BL6J strains of mice at 6 to 8 weeks of were s.c. engrafted with 2 x 10^{6} LLC1 on the right flank of mice. On day 7, 1 x 10^{6} TILs, CD8^{+}CD103^{-} PBMC,

or cTRLs ($CD8^+CD103^+$) were injected intraverscularly (i.v.). All mice received the injection of 10 μg IL-2 injection on day 8, 9 and 10.

For MC-38 models, female Rag1KO C57/BL6J strains of mice (B6.129S7-Rag1^{tm1Mom}/J, 002216, Jackson) or CD45.1 C57BL6J mice at 6 to 8 weeks of age were s.c. engrafted with 5 x 10^6 MC-38 cells on the right flank of mice. On day 7, some groups of mice received 1 x 10^6 cTRLs ($CD8^+CD103^+$) i.v. All mice received the injection of 10 μg IL-2 on day 8, 9, and 10. Some groups of mice received the intraperitoneal injection (i.p.) injection of 10 mg·kg^{-1} anti mPD-1 antibody (*In vivo* grade, BE0273, BioXCell, UK) every 2 days for 2 weeks. For the MC-38 rechallenge models, naïve or cured CD45.1 C57BL6J mice at 18 to 20 weeks of age were s.c. engrafted with 10 x 10^6 MC38 cells on the left flank of mice.

For AE17 models, female CD45.1 C57BL6J mice at 6 to 8 weeks of age were s.c. engrafted with 3 x 10^6 AE17 cells on the right flank of mice. On day 7, some groups of mice received 1 x 10^6 cTRLs ($CD8^+CD103^+$) i.v. All mice received the injection of 10 μg IL-2 on day 8, 9, and 10. Some groups of mice received the intraperitoneal injection (i.p.) injection of 10 mg·kg^{-1} anti mGITR antibody (*In vivo* grade, BE0063, BioXCell) every 3 days for 2 weeks.

Tumour growth was monitored twice a week starting from day 5 for 40 days. Tumour size was measured by a caliper using the modified ellipsoid formula: 0.5*(Length*Width^2). Mice were euthanized when the tumour size exceeds the ethical limits (> 1000mm^3). At the endpoint, tumours were isolated, fixed by 10% formalin (HT501320, Sigma), paraffin-embedded, sectioned with 5 μm thickness, and stained by anti CD8α, CD45R, CD4 and CD208 antibody (See Table. S5 for details) for immunohistochemical analysis of the degree of infiltration. Stained slides were whole-slide scanned by an Aperio digital slide scanner (Leica, Wetzlar, Germany) and quantified by Halo software (Version 3.0311, Indica Labs, Albuquerque, NM) for the number of infiltrated cells ($CD4^+$ or $CD8^+$ for T cells, $CD45R^+$ for B cells, $CD208^+$ for dentritic cells) in solid tumours using build-in random forest classifier and cytonuclear analyser (Version 2.0, Indica Labs).

For 4T1-Luc2 model, female NU/J (002019, Jackson) strains of mice at 6 to 8 weeks of age were i.v. engrafted with 2 x 10^5 4T1-Luc2 cells. On day 10, mice received 1 x 10^6 cTRLs ($CD8^+CD103^+$) or $CD8^+CD103^-$ PBMC cells i.v. All mice received the injection of 10 μg IL-2 on day 11, 12, and 13. Growth of metastasis was monitored twice a week starting from day 9 by bioluminescence (IVIS Spectrum, 124262, Perkin Elmer, Waltham, MA). Mice were i.p. injected with 3 mg of D-Luciferin potassium salt (LUCK-100, GoldBio, St. Louis, MO) 10 – 15 min prior to imaging as determined by the standard curve of Luciferin. 1 – 120s exposure with medium or low binning was used for the image acquiring. Acquired data were procesed by the IVIS Live Imaging software (Perkin Elmer) following the manufacturer's protocol. To quantify the exact of metastases, lungs were isolated at the end point from different groups. Collected lungs were fixed by 10% formalin, paraffin-embedded, sectioned and H&E stained. Stained slides were submitted to the Centre of Phenogenomics at the Mount Sinai Hospital (Toronto, Canada) for histopathology. Slides were evaluated by licensed veterinary pathologists and the exact number of micro metastases per layer were reported.

Ethics statement and patient samples. For colorectal cancer samples, the dissociated tumour samples and paired PBMC were purchased from Discovery Life Science (DLS, Hutsville, AL). The cases we purchased were at stage II – III with more than 40% $CD45^+$ cells in dissociated tumour samples. Basic information and percentage of $CD45^+$ cells of each sample was examined by DLS at the time of bankding and provided as a PDF sheet.

For lung cancer samples, all experiments were approved by the Research Ethics Board (REB) at the Toronto General Hospital Research Institute (TGHRI). All individuals have provided written consent and the protocol was approved by the TGHRI. All blood samples were collected in standard K2-EDTA tubes (02-657-32, BD) and stored in 2 – 8 ^{o}C for up to 6 hrs before gradient centrifuge in Ficoll Paque (GE17-1440-02, Sigma). Isolated PBMCs were stored in CryoStor CS10 freezing medium (07930, Stem Cell Technologies, Canada) under a liquid nitrogen condition before use. Resected tumour were dissociated using a human tissue dissociation kit (130-095-929, Miltenyi), filtered twice through 100 μm stainers, and cryopreserved in liquid nitrogen before use. Maglianant pleural effusions (MPE) were obtained via thoracentesis, lysed by RBC lysis buffer, and filtered twice through 100 μm stainers and cryopreserved in liquid nitrogen before use.
For TCR sequencing, $CD8^+$ T cells in cryopreserved dissociated tumour cells (DTCs) were enriched by CD8-mediated MATIC following the protocol described in the section 'chip fabrication and operation'. $CD8^+CD103^-$ and $CD8^+CD103^+$ cells were purified from cryopreserved PBMCs using MATIC following the same protocol. Isolated cells were centrifuged to form cell pellets for downstream sequencing.

For the co-culture experiments, leukocytes in DTCs were depleted by the MACS-mediated selection against CD45 using LD columns (130-042-901, Miltenyi) using the QuadroMACS separator. $CD8^+CD103^+$ cells were purified from cryopreserved PBMCs using MATIC following the protocol described in the section of 'chip

fabrication and operation'. Bulk or purified cells were co-cultured with leukocyte-depleted DTCs for 12 - 24 hrs in the medium consisting 50% of IMDM, 50% of ImmunoCult-XF T cell expansion medium (10981, Stem Cell Technologies), 5% human AB serum (BP2525100, Fisher Scientific, Waltham, MA), 250 - 500 ng/mL recombinant human interleukin 2 (78036.2, Stem Cell Technologies), 1% Penicillin/Streptomycin (15140122, Thermo) and 5 μg/mL Brefeldin A (B7651, Sigma). The percentage of interferon gamma (IFN-γ) secreting cells was assessed by the flow cytometry by gating the populations of $CD8^+/IFN\text{-}\gamma^+$.

Statistical analysis. Results were shown by Prism GraphPad (Version 9.1.0, GraphPad Software, San Diego, CA) as an average ± standard deviation unless specified elsewhere. Each dot represents a biological replicate. P value was calculated by the build-in analysis function of Prism GraphPad.

Reporting Summary. Further information on research design is available in the Nature Research Reporting Summary linked to this article.

Data availability

The main data supporting the results in this study are available within the paper and its Supplementary Information. The RNAseq data is available from the gene expression omnibus (GEO, https://www.ncbi.nlm.nih.gov/geo/) under the access code **CODE**. The unprocessed TCR sequencing files and CyTOF data are too large to be publicly shared, yet they are available from the corresponding author on reasonable request. Source data are provided with this paper.

References

1. Rosenberg, S. A. Cell transfer immunotherapy for metastatic solid cancer—what clinicians need to know. *Nat. Rev. Clin. Oncol.* **8**, 577–585 (2011).
2. Gong, N., Sheppard, N. C., Billingsley, M. M., June, C. H. & Mitchell, M. J. Nanomaterials for T-cell cancer immunotherapy. *Nat. Nanotechnol.* **16**, 25–36 (2021).
3. Andersen, R. *et al.* Long-Lasting Complete Responses in Patients with Metastatic Melanoma after Adoptive Cell Therapy with Tumor-Infiltrating Lymphocytes and an Attenuated IL2 Regimen. *Clin. Cancer Res.* **22**, 3734–3745 (2016).
4. van den Berg, J. H. *et al.* Tumor infiltrating lymphocytes (TIL) therapy in metastatic melanoma: boosting of neoantigen-specific T cell reactivity and long-term follow-up. *J. Immunother. Cancer* **8**, e000848 (2020).
5. Veatch, J. R., Simon, S. & Riddell, S. R. Tumor-infiltrating lymphocytes make inroads in non–small-cell lung cancer. *Nat. Med.* **27**, 1338–1339 (2021).
6. Andersen, R. *et al.* T-cell Responses in the Microenvironment of Primary Renal Cell Carcinoma—Implications for Adoptive Cell Therapy. *Cancer Immunol. Res.* **6**, 222–235 (2018).
7. Stevanović, S. *et al.* Complete Regression of Metastatic Cervical Cancer After Treatment With Human Papillomavirus–Targeted Tumor-Infiltrating T Cells. *J. Clin. Oncol.* **33**, 1543–1550 (2015).
8. Zacharakis, N. *et al.* Breast Cancers Are Immunogenic: Immunologic Analyses and a Phase II Pilot Clinical Trial Using Mutation-Reactive Autologous Lymphocytes. *J. Clin. Oncol.* JCO.21.02170 (2022) doi:10.1200/JCO.21.02170.
9. Dijkstra, K. K. *et al.* Generation of Tumor-Reactive T Cells by Co-culture of Peripheral Blood Lymphocytes and Tumor Organoids. *Cell* **174**, 1586-1598.e12 (2018).
10. Chen, F. *et al.* Neoantigen identification strategies enable personalized immunotherapy in refractory solid tumors. *J. Clin. Invest.* **129**, 2056–2070 (2019).
11. van Rooij, N. *et al.* Tumor Exome Analysis Reveals Neoantigen-Specific T-Cell Reactivity in an Ipilimumab-Responsive Melanoma. *J. Clin. Oncol.* **31**, e439–e442 (2013).
12. Rizvi, N. A. *et al.* Mutational landscape determines sensitivity to PD-1 blockade in non–small cell lung cancer. *Science* **348**, 124–128 (2015).
13. Gros, A. *et al.* Prospective identification of neoantigen-specific lymphocytes in the peripheral blood of melanoma patients. *Nat. Med.* **22**, 433–438 (2016).
14. Cohen, C. J. *et al.* Isolation of neoantigen-specific T cells from tumor and peripheral lymphocytes. *J. Clin. Invest.* **125**, 3981–3991 (2015).
15. Peng, S. *et al.* Sensitive Detection and Analysis of Neoantigen-Specific T Cell Populations from Tumors and Blood. *Cell Rep.* **28**, 2728-2738.e7 (2019).
16. Bobisse, S. *et al.* Sensitive and frequent identification of high avidity neo-epitope specific CD8 + T cells in immunotherapy-naive ovarian cancer. *Nat. Commun.* **9**, 1092 (2018).
17. Martin, S. D. *et al.* A library-based screening method identifies neoantigen-reactive T cells in peripheral blood prior to relapse of ovarian cancer. *OncoImmunology* **7**, e1371895 (2018).

18. Valpione, S. *et al.* Immune awakening revealed by peripheral T cell dynamics after one cycle of immunotherapy. *Nat. Cancer* **1**, 210–221 (2020).
19. Kamphorst, A. O. *et al.* Proliferation of PD-1+ CD8 T cells in peripheral blood after PD-1–targeted therapy in lung cancer patients. *Proc. Natl. Acad. Sci.* **114**, 4993–4998 (2017).
20. Holm, J. S. *et al.* Neoantigen-specific CD8 T cell responses in the peripheral blood following PD-L1 blockade might predict therapy outcome in metastatic urothelial carcinoma. *Nat. Commun.* **13**, 1935 (2022).
21. Wang, Z. Efficient recovery of potent tumour-infiltrating lymphocytes through quantitative immunomagnetic cell sorting. *Nat. Biomed. Eng.* 19 doi:10.1038/s41551-021-00820-y.
22. Fehlings, M. *et al.* Late-differentiated effector neoantigen-specific CD8+ T cells are enriched in peripheral blood of non-small cell lung carcinoma patients responding to atezolizumab treatment. *J. Immunother. Cancer* **7**, 249 (2019).
23. Li, Z. *et al.* In vivo labeling reveals continuous trafficking of TCF-1+ T cells between tumor and lymphoid tissue. *J. Exp. Med.* **219**, e20210749 (2022).
24. Roberts, A. D., Ely, K. H. & Woodland, D. L. Differential contributions of central and effector memory T cells to recall responses. *J. Exp. Med.* **202**, 123–133 (2005).
25. Wang, Z. *et al.* Ultrasensitive and rapid quantification of rare tumorigenic stem cells in hPSC-derived cardiomyocyte populations. *Sci. Adv.* **6**, eaay7629 (2020).
26. Wang, Z., Sargent, E. H. & Kelley, S. O. Ultrasensitive Detection and Depletion of Rare Leukemic B Cells in T Cell Populations via Immunomagnetic Cell Ranking. *Anal. Chem.* **93**, 2327–2335 (2021).
27. Allan, A. L. & Keeney, M. Circulating Tumor Cell Analysis: Technical and Statistical Considerations for Application to the Clinic. *J. Oncol.* **2010**, 1–10 (2010).
28. Hedley, B. D. & Keeney, M. Technical issues: flow cytometry and rare event analysis. *Int. J. Lab. Hematol.* **35**, 344–350 (2013).
29. Faraghat, S. A. *et al.* High-throughput, low-loss, low-cost, and label-free cell separation using electrophysiology-activated cell enrichment. *Proc. Natl. Acad. Sci.* **114**, 4591–4596 (2017).
30. Sutermaster, B. A. & Darling, E. M. Considerations for high-yield, high-throughput cell enrichment: fluorescence versus magnetic sorting. *Sci. Rep.* **9**, 227 (2019).
31. Labib, M. *et al.* Tracking the expression of therapeutic protein targets in rare cells by antibody-mediated nanoparticle labelling and magnetic sorting. *Nat. Biomed. Eng.* **5**, 41–52 (2021).
32. Wang, Z. *et al.* Nanoparticle Amplification Labeling for High-Performance Magnetic Cell Sorting. *Nano Lett.* acs.nanolett.2c01018 (2022) doi:10.1021/acs.nanolett.2c01018.
33. Carlisle, M. L., King, M. R. & Karp, D. R. g-Glutamyl transpeptidase activity alters the T cell response to oxidative stress and Fas-induced apoptosis. *Int. Immunol.* **15**, 17 (2003).
34. Xiao, Z., Mescher, M. F. & Jameson, S. C. Detuning CD8 T cells: down-regulation of CD8 expression, tetramer binding, and response during CTL activation. *J. Exp. Med.* **204**, 2667–2677 (2007).
35. Wong, M. T. *et al.* A High-Dimensional Atlas of Human T Cell Diversity Reveals Tissue-Specific Trafficking and Cytokine Signatures. *Immunity* **45**, 442–456 (2016).
36. Corgnac, S. *et al.* CD103+CD8+ TRM Cells Accumulate in Tumors of Anti-PD-1-Responder Lung Cancer Patients and Are Tumor-Reactive Lymphocytes Enriched with Tc17. *Cell Rep. Med.* **1**, 100127 (2020).
37. Banchereau, R. *et al.* Intratumoral CD103+ CD8+ T cells predict response to PD-L1 blockade. *J. Immunother. Cancer* **9**, e002231 (2021).
38. Duhen, T. *et al.* Co-expression of CD39 and CD103 identifies tumor-reactive CD8 T cells in human solid tumors. *Nat. Commun.* **9**, 2724 (2018).
39. Park, S. L., Gebhardt, T. & Mackay, L. K. Tissue-Resident Memory T Cells in Cancer Immunosurveillance. *Trends Immunol.* **40**, 735–747 (2019).
40. Klicznik, M. M. *et al.* Human CD4 $^{+}$ CD103 $^{+}$ cutaneous resident memory T cells are found in the circulation of healthy individuals. *Sci. Immunol.* **4**, eaav8995 (2019).
41. Fonseca, R. *et al.* Developmental plasticity allows outside-in immune responses by resident memory T cells. *Nat. Immunol.* **21**, 412–421 (2020).
42. Schlickum, S. *et al.* Integrin αE(CD103)β7 influences cellular shape and motility in a ligand-dependent fashion. *Blood* **112**, 619–625 (2008).
43. Mattila, P. K. & Lappalainen, P. Filopodia: molecular architecture and cellular functions. *Nat. Rev. Mol. Cell Biol.* **9**, 446–454 (2008).
44. Abd Hamid, M. *et al.* Self-Maintaining CD103 $^{+}$ Cancer-Specific T Cells Are Highly Energetic with Rapid Cytotoxic and Effector Responses. *Cancer Immunol. Res.* **8**, 203–216 (2020).
45. Dudley, M. E., Wunderlich, J. R., Shelton, T. E., Even, J. & Rosenberg, S. A. Generation of Tumor-Infiltrating Lymphocyte Cultures for Use in Adoptive Transfer Therapy for Melanoma Patients: *J. Immunother.* **26**, 332–342 (2003).
46. Carmona, S. J., Siddiqui, I., Bilous, M., Held, W. & Gfeller, D. Deciphering the transcriptomic landscape of tumor-infiltrating CD8 lymphocytes in B16 melanoma tumors with single-cell RNA-Seq. *OncoImmunology* **9**, 1737369 (2020).

47. Miller, B. C. *et al.* Subsets of exhausted CD8+ T cells differentially mediate tumor control and respond to checkpoint blockade. *Nat. Immunol.* **20**, 326–336 (2019).
48. Good, C. R. *et al.* An NK-like CAR T cell transition in CAR T cell dysfunction. *Cell* **184**, 6081-6100.e26 (2021).
49. Zheng, L. *et al.* Pan-cancer single-cell landscape of tumor-infiltrating T cells. *Science* **374**, abe6474 (2021).
50. Ma, Q., Wang, Y., Lo, A. S.-Y., Gomes, E. M. & Junghans, R. P. Cell Density Plays a Critical Role in Ex Vivo Expansion of T Cells for Adoptive Immunotherapy. *J. Biomed. Biotechnol.* **2010**, 1–13 (2010).
51. Amsen, D., van Gisbergen, K. P. J. M., Hombrink, P. & van Lier, R. A. W. Tissue-resident memory T cells at the center of immunity to solid tumors. *Nat. Immunol.* **19**, 538–546 (2018).
52. Szabo, P. A., Miron, M. & Farber, D. L. Location, location, location: Tissue resident memory T cells in mice and humans. *Sci. Immunol.* **4**, eaas9673 (2019).
53. Wang, Z.-Q. *et al.* CD103 and Intratumoral Immune Response in Breast Cancer. *Clin. Cancer Res.* **22**, 6290–6297 (2016).
54. Djenidi, F. *et al.* CD8 $^{+}$ CD103 $^{+}$ Tumor–Infiltrating Lymphocytes Are Tumor-Specific Tissue-Resident Memory T Cells and a Prognostic Factor for Survival in Lung Cancer Patients. *J. Immunol.* **194**, 3475–3486 (2015).
55. Komdeur, F. L. *et al.* CD103+ tumor-infiltrating lymphocytes are tumor-reactive intraepithelial CD8+ T cells associated with prognostic benefit and therapy response in cervical cancer. *OncoImmunology* **6**, e1338230 (2017).
56. Xiao, Y. *et al.* CD103 $^{+}$ T and Dendritic Cells Indicate a Favorable Prognosis in Oral Cancer. *J. Dent. Res.* **98**, 1480–1487 (2019).
57. Li, T. *et al.* TIMER2.0 for analysis of tumor-infiltrating immune cells. *Nucleic Acids Res.* **48**, W509–W514 (2020).
58. Newman, A. M. *et al.* Robust enumeration of cell subsets from tissue expression profiles. *Nat. Methods* **12**, 453–457 (2015).
59. Jiang, P. *et al.* Signatures of T cell dysfunction and exclusion predict cancer immunotherapy response. *Nat. Med.* **24**, 1550–1558 (2018).
60. Kim, Y., Shin, Y. & Kang, G. H. Prognostic significance of CD103+ immune cells in solid tumor: a systemic review and meta-analysis. *Sci. Rep.* **9**, 3808 (2019).
61. Guedan, S., Ruella, M. & June, C. H. Emerging Cellular Therapies for Cancer. *Annu. Rev. Immunol.* **37**, 145–171 (2019).
62. Krishna, S. *et al.* Stem-like CD8 T cells mediate response of adoptive cell immunotherapy against human cancer. *Science* **370**, 1328–1334 (2020).
63. Leko, V. *et al.* Identification of neoantigen-reactive T lymphocytes in the peripheral blood of a patient with glioblastoma. *J. Immunother. Cancer* **9**, e002882 (2021).
64. Melenhorst, J. J. *et al.* Decade-long leukaemia remissions with persistence of CD4+ CAR T cells. *Nature* **602**, 503–509 (2022).
65. Lawson, K. A. *et al.* Functional genomic landscape of cancer-intrinsic evasion of killing by T cells. *Nature* **586**, 120–126 (2020).

Acknowledgements

We would like to thank T. Chen at the Centre for Advanced Single Cell Analysis (CASCA), Sick Children Hospital, Toronto for her help in CyTOF, N. Simard at the centralize flow cytometry facility at Temerty Faculty of Medicine, University of Toronto for her help in FACS sorting, A.C. Zhou at the Medicine by Design initiative at the University of Toronto for her comments, W. Xiao and A. Archila at the University Health Network (UHN) for their help in tail vein injection, M. Peralta at the UHN PRP facility and N. Law at the UHN STTARR facility for their help in immunohistochemistry, J. Jonkman at the UHN AOMF facility for his help in image quantitation, J. Wei and J. Moffat at the Terrence Donnelly Centre, University of Toronto for donating $CT26^{HA}$ and OT-1 cells. This study was supported in part by the Canadian Institutes of Health Research (grant no. FDN-148415) and the Collaborative Health Research Projects program (CIHR/NSERC partnered). This research is also part of the University of Toronto's Medicine by Design initiative, which receives funding from the Canada First Research Excellence Fund. The study was also supported in part by the McCormick Catalyst Fund at Northwestern University.

Author contributions

Z.W and S.O.K conceived and designed the experiments. Z.W performed cell isolation, flow cytometry and CyTOF. S.A performed the animal study. M.L performed RNA extraction and qPCR. H.W extracted the OVA plasmid and assisted with the animal study. L.W maintained the AE17 cell lines. L.W, F.B-Z, N.S, S.B and S.K managed patient-sample collection, distribution and administration. All authors discussed the results, analysed the data and contributed to the preparation and editing of the manuscript.

Competing interests

S.O.K and Z.W have a filled patent application using parts of the data reported in this article. S.O.K has a patent “Device for capture of particles in a flow” US10073079 licensed to Cellular Analytics. A.J.R.M is a paid consultant for Cellular Analytics. M.D.P. received personal fees from Actelion, AstraZeneca, Bayer, Bristol Myers Squibb, Merck, and Roche outside of the submitted work. S.O.K received research funds from Amgen through a sponsored research agreement. The other authors declare no competing interests.

Additional information

Extended data is available for this paper at https://doi.org/10.1038/s41551-02X-XXXX-X.

Supplementary information The online version contains supplementary material available at https://doi.org/10.1038/s41551-02X-XXXX-X.

Correspondence and requests for materials should be addressed to Shana Kelley.

Peer review information *Nature Biomedical Engineering* thanks Rong Fan, Alexandre Harari and Paul Robbins for their contribution to the peer review of this work. Peer reviewer reports are available.

Fig. 1 | Non-invasive collection of tumour-reactive cells in blood circulation for cancer immunotherapy. a, Schematic showing conventional invasive TIL therapy (left, it requires excisional surgery to obtain large tumour lesion) compared to non-invasive circulating tumour-reactive lymphocytes (cTRL) therapy (right, it requires blood collection only). **b**, Schematic showing the trafficking dynamics of cTRLs between tumours.

Fig. 2 | Isolation of tumour-reactive TRLs in blood circulation. a, Working principle of tumour reactivity-mediated microfluidic cell sorting for analysis. Cells were firstly magnetically labelled based on their TCR reactivity with tumour antigen-derived MHC multimers. Magnetically labelled cells were separated from their counterparts by microfluidic cell sorting for downstream analysis. **b**, Workflow of the identification via defined epitope models. $CD8^+$ T cells in PBMC were classified as tumour-reactive and non-reactive populations based on their reactivity with multimers. Classified cells were compared to intratumoural $CD8^+$ TILs for clonal analysis. **c**, Quantitation of the sorting performance based on antibody and multimer through microfluidic sorting. **d**, Comparison of clonal similarity among TIL, cTRL, and PBMC by V-J usage profile. **e**, Analyses of the coverage of top 50 clones between each population. Unpaired t-test, mean ± s.d., each dot represents a biological replicate.

Fig. 3 | Molecular and phenotypic signature of cTRL during and post migration. a, Volcano plots showing the differential expression (DE) of genes when comparing the normalized counts from non-cTRL $CD8^+$ PBMC and cTRL identified by multimer-based sorting from the B16 model. Key genes for $CD8^+$ T cells were presented as a heatmap alongside. **b**, Identification of tumour-reactivity in circulating $CD8^+CD103^+$ populations. **c**, Quantitation of tumour-reactive fraction in circulating $CD8^+CD103^+$ populations. **d**, CyTOF analysis of multimer-binding cTRLs. The expression levels of CD103, CD39, PD-1, and CD69 were examined. **e**, Quantitation of the expression level of CD103, CD39, PD-1 and CD69 in cTRLs during migration. **f**, CyTOF analysis of $CD45.2^+$ cTRLs and $CD45.1^+$ TILs for the expression of CD103 in AE17 models. **g**, Quantitation of CyTOF data for the expression of CD103, CD69 and PD-1 in $CD45.2^+$ cTRLs and $CD45.1^+$ TILs. Unpaired t-test, mean ± s.d., each dot represents a biological replicate.

Fig. 4 | cTRLs exhibit significant levels of activity against primary and metastasized tumours in murine models. a, Workflow of the animal study. cTRL, $CD8^+CD103^-$ PBMC and TIL were expanded 1 – 2 weeks *in vitro* before adoptive cell transfer. IL-2 was given daily for the first 3 days post cell transfer to boost lymphocyte proliferation. **b**, Quantitation of tumour size, survival rate, and percentage of infiltrated $CD8^+$ cells in s.c. B16 models WT C57BL6 mice treated by different T cells (n = 5). **c**, Representative bioluminescence images treated by different T cells (n = 6) in induced 4T1 metastasis models in nude mice. **d**, Quantitation of the total flux and survival rate in induced 4T1 metastasis models. Unpaired t-test, mean ± s.d., each dot represents a biological replicate.

Fig. 5 | Synergistic effects of cTRLs and ICB/costimulatory molecules. a, Quantitation of tumour size, survival rate, and percentage of infiltrated $CD8^+$ cells in s.c. MC38 models treated by different therapeutic modalities (n = 5). **b**, Enriched pathways from upregulated RNAs reveal that αPD-1 and cTRLs generate different impacts to the immune responses within the tumour microenvironment in s.c. MC38 models. **c**, Quantitation of $CD4^+$ T cells and $CD208^+$ dendritic cells post different therapeutic modalities. **d**, Rapid tumour rejection and formation of long-lasting TRLs were observed in cTRL-cured mice. **e**, Quantitation of tumour size, survival rate, and percentage of infiltrated $CD8^+$ cells in s.c. AE17 models treated by different therapeutic modalities (n = 5). **f**, Quantitation of lymphocyte subpopulations at the endpoint of treatment in endogenous ($CD45.1^+$) populations in s.c. AE17 models. **g**, Quantitation of CD103 expression in transferred cTRLs ($CD45.2^+$) and endogenous lymphocytes ($CD45.1^+$) in s.c. AE17 models. Unpaired t-test, mean ± s.d., each dot represents a biological replicate.

Fig. 6 | $CD103^+$ defines cTRL population in human PBMC. a, Workflow of the co-culture assay to study the relationship between tumour-reactivity and CD103 on human PBMCs. **b**, Representative flow cytometric profile of IFN-γ secreting populations according to CD103 expression. This specific set of images is from PE95. **c**, Quantitation of IFN-γ secreting populations in CD8+CD103+ and CD8+CD103- cells across the patient cohort of malignant pleural effusion (MPE). Unpaired t-test, mean ± s.d., each dot represents a technical replicate.

Fig. 7 | $CD8^+CD103^+$ cTRLs are phenotypically and clonally tumour-specific. a, Workflow of the co-culture assay to examine the level of tumour specificity of isolated cTRLs. **b**, Representative flow cytometric profile of IFN-γ secreting populations in co-cultured populations. This specific set of images is from PE86. **c**, Quantitation of IFN-γ secreting populations across a set of 18 patient samples. Tumour cells used in a co-culture model to induce IFN-γ secretion were harvested either from tumour tissue (red) or malignant pleural effusions (blue). Fold enrichment was calculated by comparing the percentage of IFNγ+ cells in bulk CD8+ and CD8+CD103+ populations post co-culture. **d**, Analysis of the coverage of top 50 TIL clones in cTRLs

and PBMC populations among 3 colon cancer patients (CA01 – CA03). **e**, Comparison of clonal similarity among TILs, cTRLs and PBMC by V-J usage profile. cTRLs contains four TIL-derived major clones. Unpaired t-test, mean ± s.d. For **c**, each dot represents a technical replicate. For **d**, each dot represents a biological replicate.

Table 1 | Fraction of top-20 TIL clones (by abundance) in cTRL and non-cTRL CD8+ PBMC.

CDR3 sequence	Fraction in TIL	Fraction in cTRL	Fraction in non-cTRL $CD8^+$ PBMC
CAASVSGSFNKLTF	1.68%	0.06%	ND*
CAVSEAGSFNKLTF	1.29%	5.22%	ND
CAWSLSGTTSAETLYF	1.20%	ND	ND
CTCSADLGGFYAEQFF	1.19%	0.19%	ND
CTCSADRGGGYAEQFF	1.03%	3.98%	ND
CAMERPSSGQKLVF	1.01%	ND	ND
CAMREGGSNAKLTF	1.00%	1.20%	ND
CATDINQGGSAKLIF	0.99%	1.23%	ND
CAMREGMPNYNVLYF	0.88%	1.17%	ND
CAMREGGTGGYKVVF	0.86%	0.39%	ND
CAMSTGNYKYVF	0.80%	4.83%	0.07%
CASGVSGPDYTF	0.77%	1.14%	ND
CAVNTGNYKYVF	0.70%	0.15%	ND
CAVSMPSGSWQLIF	0.66%	ND	ND
CAMREANTGANTGKLTF	0.62%	4.92%	ND
CILRVDGPNYNVLYF	0.55%	1.07%	ND
CASNQGGSAKLIF	0.54%	1.40%	ND
CAAINNYAQGLTF	0.54%	1.14%	ND
CAMREGVGSALGRLHF	0.52%	0.17%	ND
CASSDVTGAYEQYF	0.50%	0.17%	ND

*ND, Not detected.

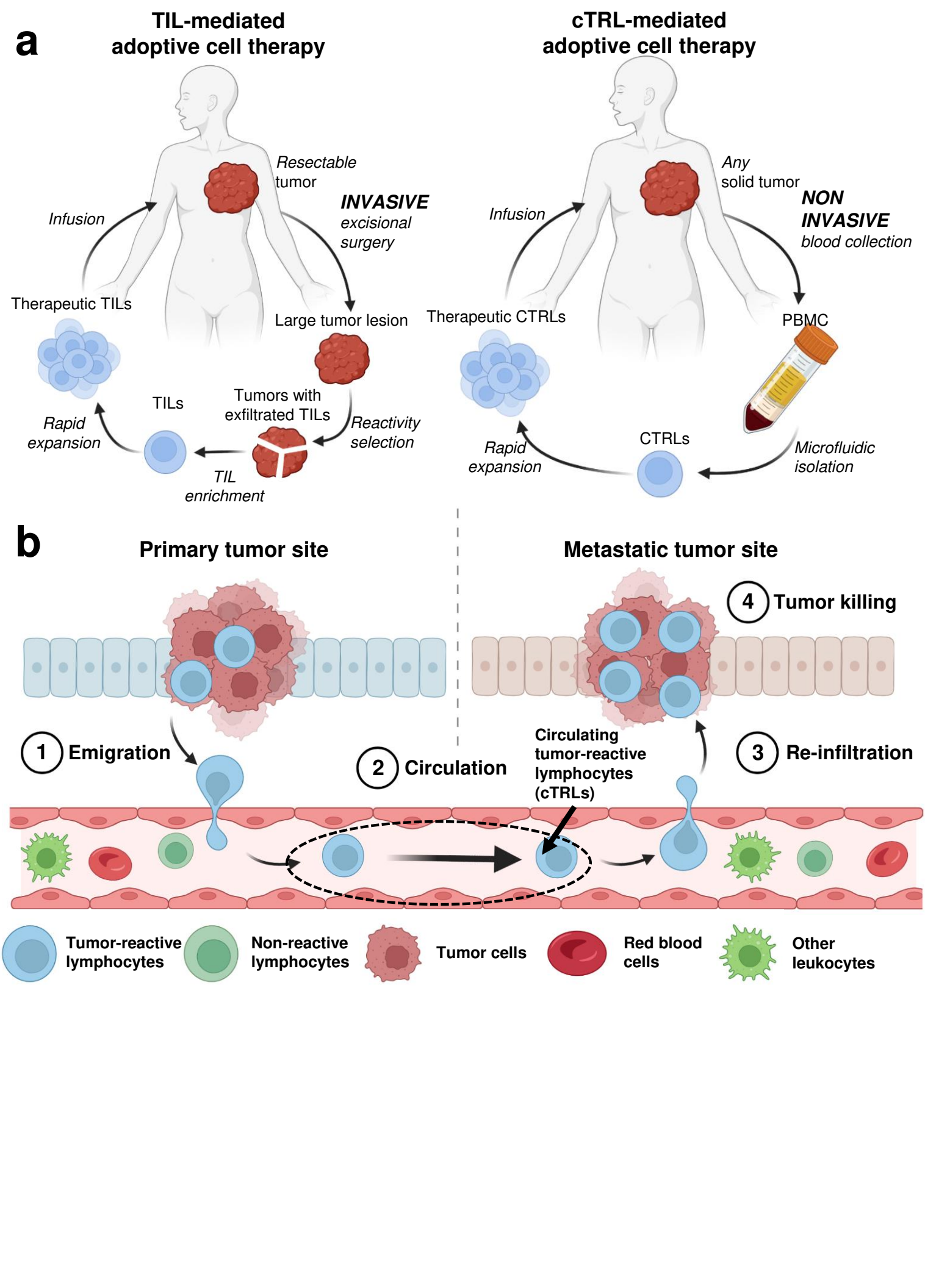
a
TIL-mediated adoptive cell therapy
Resectable tumor
INVASIVE excisional surgery
Infusion
Therapeutic TILs
Large tumor lesion
Tumors with exfiltrated TILs
Reactivity selection
TILs
Rapid expansion
TIL enrichment
cTRL-mediated adoptive cell therapy
Any solid tumor
NON INVASIVE blood collection
Infusion
Therapeutic CTRLs
PBMC
CTRLs
Rapid expansion
Microfluidic isolation
b
Primary tumor site
Metastatic tumor site
4 Tumor killing
1 Emigration
2 Circulation
Circulating tumor-reactive lymphocytes (cTRLs)
3 Re-infiltration
Tumor-reactive lymphocytes
Non-reactive lymphocytes
Tumor cells
Red blood cells
Other leukocytes

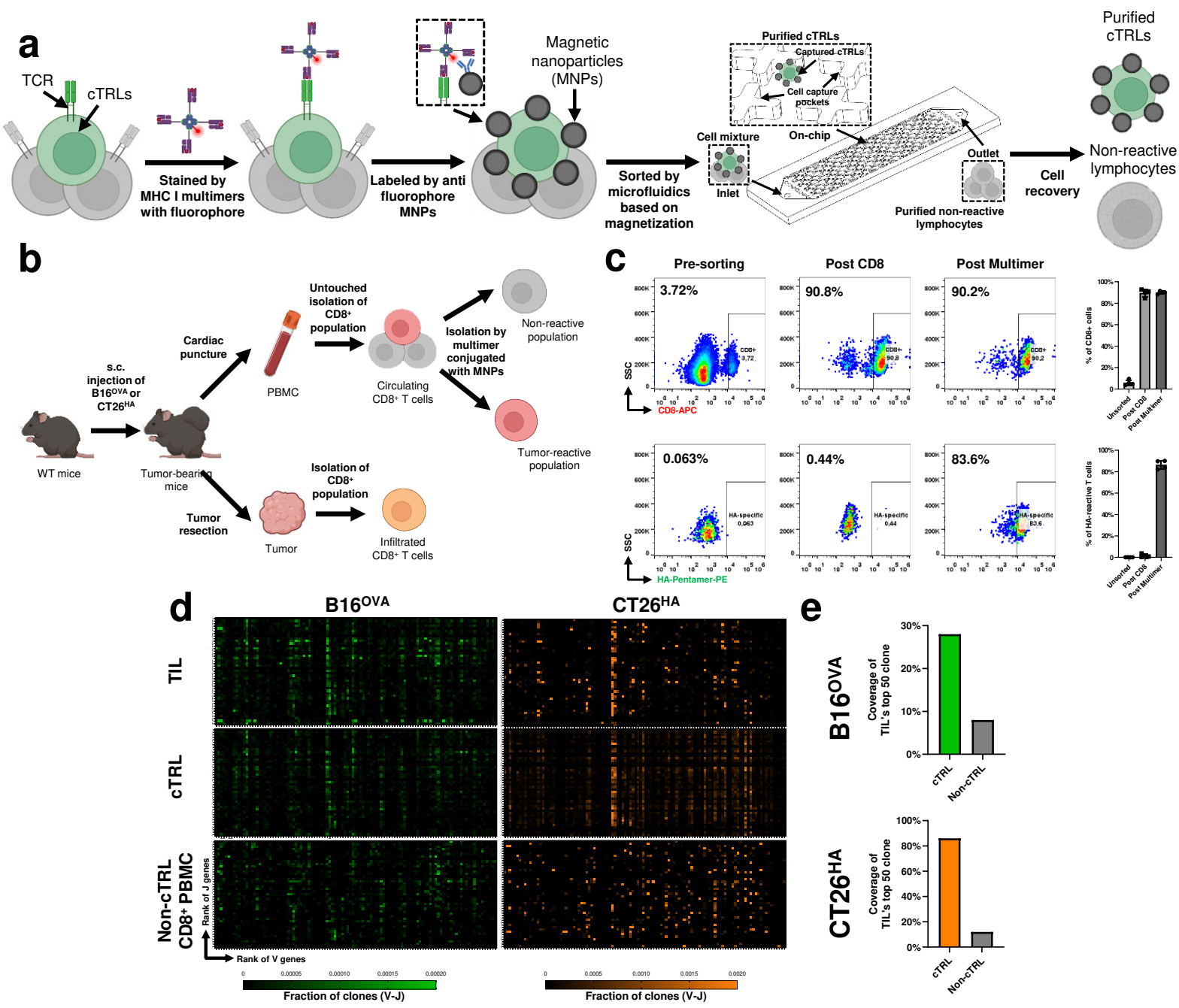
a
TCR
cTRLs
Stained by MHC I multimers with fluorophore
Magnetic nanoparticles (MNPs)
Labeled by anti fluorophore MNPs
Sorted by microfluidics based on magnetization
Purified cTRLs
Captured cTRLs
Cell capture pockets
Cell mixture
On-chip
Inlet
Outlet
Purified non-reactive lymphocytes
Cell recovery
Purified cTRLs
Non-reactive lymphocytes
b
WT mice
s.c. injection of B16OVA or CT26HA
Tumor-bearing mice
Cardiac puncture
PBMC
Untouched isolation of CD8+ population
Circulating CD8+ T cells
Isolation by multimer conjugated with MNPs
Non-reactive population
Tumor-reactive population
Tumor resection
Tumor
Isolation of CD8+ population
Infiltrated CD8+ T cells
c
Pre-sorting
Post CD8
Post Multimer
3.72%
90.8%
90.2%
SSC
CD8-APC
% of CD8+ cells
Unsorted
Post CD8
Post Multimer
0.063%
0.44%
83.6%
HA-Pentamer-PE
% of HA-reactive T cells
d
B16OVA
CT26HA
TIL
cTRL
Non-cTRL CD8+ PBMC
Rank of J genes
Rank of V genes
Fraction of clones (V-J)
e
B16OVA
Coverage of TIL's top 50 clone
cTRL
Non-cTRL
CT26HA

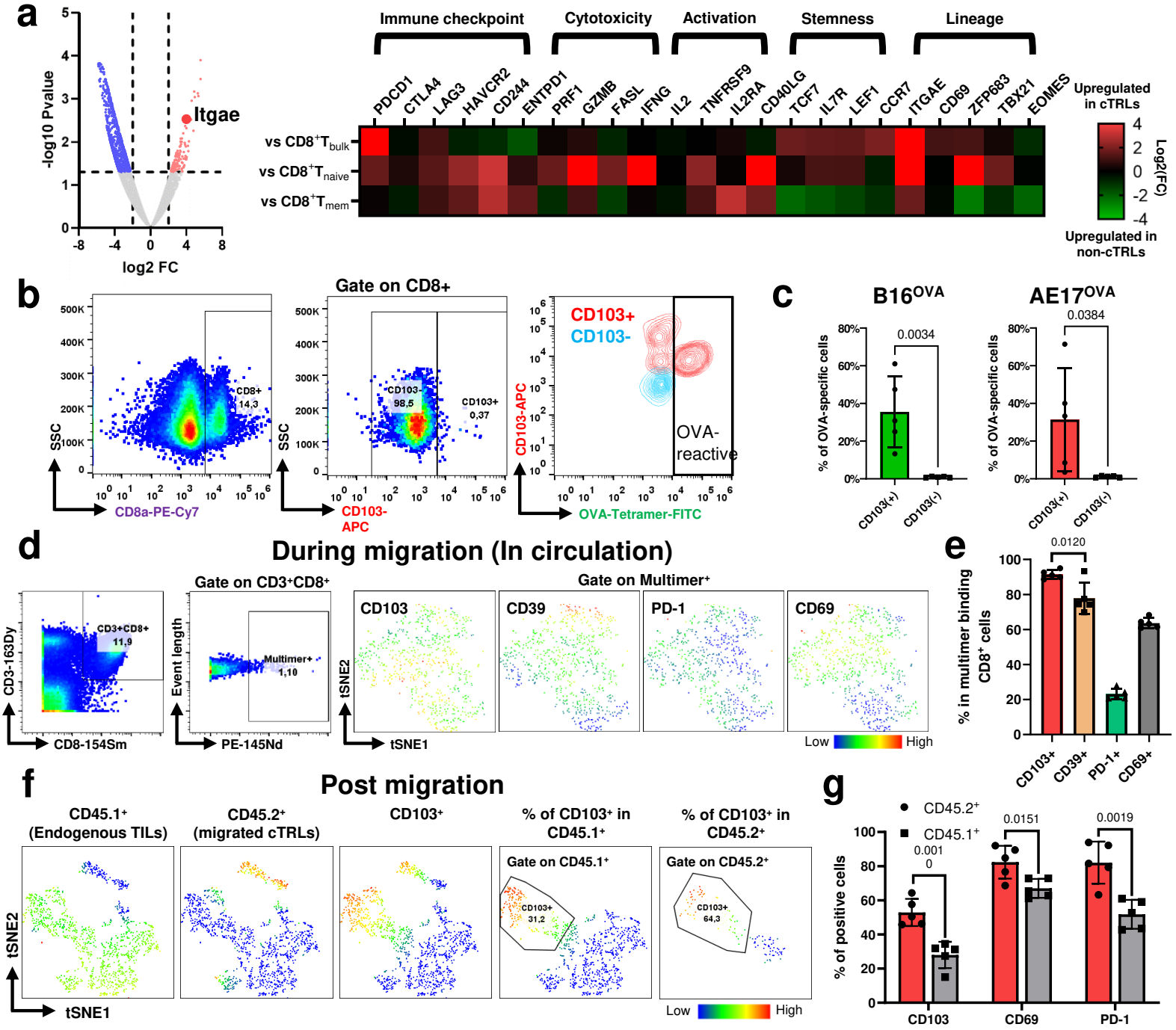
a
-log10 Pvalue
log2 FC
Itgae
Immune checkpoint
Cytotoxicity
Activation
Stemness
Lineage
PDCD1
CTLA4
LAG3
HAVCR2
CD244
ENTPD1
PRF1
GZMB
FASL
IFNG
IL2
TNFRSF9
IL2RA
CD40LG
TCF7
IL7R
LEF1
CCR7
ITGAE
CD69
ZFP683
TBX21
EOMES
vs CD8+Tbulk
vs CD8+Tnaive
vs CD8+Tmem
Upregulated in cTRLs
Log2(FC)
Upregulated in non-cTRLs
b
Gate on CD8+
SSC
CD8a-PE-Cy7
CD8+ 14,3
CD103- 98,5
CD103+ 0,37
CD103-APC
CD103+
CD103-
OVA-reactive
OVA-Tetramer-FITC
c
B16OVA
AE17OVA
0.0034
0.0384
% of OVA-specific cells
CD103(+)
CD103(-)
d
During migration (In circulation)
Gate on CD3+CD8+
Gate on Multimer+
CD3-163Dy
CD8-154Sm
CD3+CD8+ 11,9
Event length
PE-145Nd
Multimer+ 1,10
tSNE2
tSNE1
CD103
CD39
PD-1
CD69
Low
High
e
0.0120
% in multimer binding CD8+ cells
CD103+
CD39+
PD-1+
CD69+
f
Post migration
CD45.1+ (Endogenous TILs)
CD45.2+ (migrated cTRLs)
CD103+
% of CD103+ in CD45.1+
% of CD103+ in CD45.2+
Gate on CD45.1+
Gate on CD45.2+
CD103+ 31,2
CD103+ 64,3
g
CD45.2+
CD45.1+
0.001
0
0.0151
0.0019
% of positive cells
CD103
CD69
PD-1

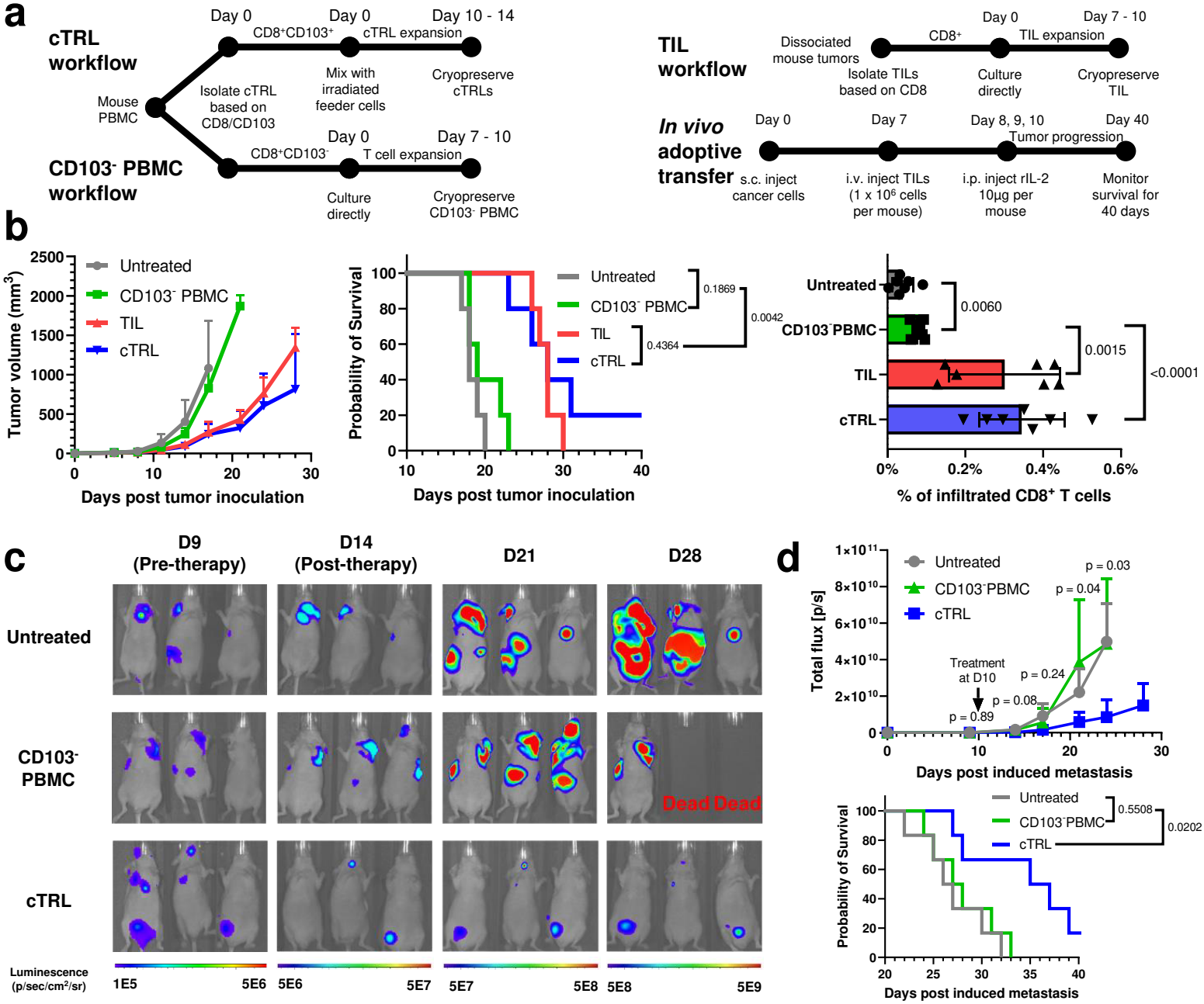
a
cTRL workflow
Day 0
CD8+CD103+
Day 0
cTRL expansion
Day 10 - 14
Mouse PBMC
Isolate cTRL based on CD8/CD103
Mix with irradiated feeder cells
Cryopreserve cTRLs
CD103- PBMC workflow
Day 0
CD8+CD103-
Day 0
T cell expansion
Day 7 - 10
Culture directly
Cryopreserve CD103- PBMC
TIL workflow
Dissociated mouse tumors
Isolate TILs based on CD8
Day 0
CD8+
Day 0
TIL expansion
Day 7 - 10
Culture directly
Cryopreserve TIL
In vivo adoptive transfer
Day 0
s.c. inject cancer cells
Day 7
i.v. inject TILs (1 x 10^6 cells per mouse)
Day 8, 9, 10
i.p. inject rIL-2 10µg per mouse
Day 40
Tumor progression
Monitor survival for 40 days
b
Tumor volume (mm3)
Days post tumor inoculation
Untreated
CD103- PBMC
TIL
cTRL
Probability of Survival
Days post tumor inoculation
0.1869
0.0042
0.4364
% of infiltrated CD8+ T cells
0.0060
0.0015
<0.0001
c
D9 (Pre-therapy)
D14 (Post-therapy)
D21
D28
Untreated
CD103- PBMC
cTRL
Dead Dead
Luminescence (p/sec/cm2/sr)
1E5
5E6
5E6
5E7
5E7
5E8
5E8
5E9
d
Total flux [p/s]
Days post induced metastasis
Treatment at D10
p = 0.89
p = 0.08
p = 0.24
p = 0.04
p = 0.03
Probability of Survival
0.5508
0.0202

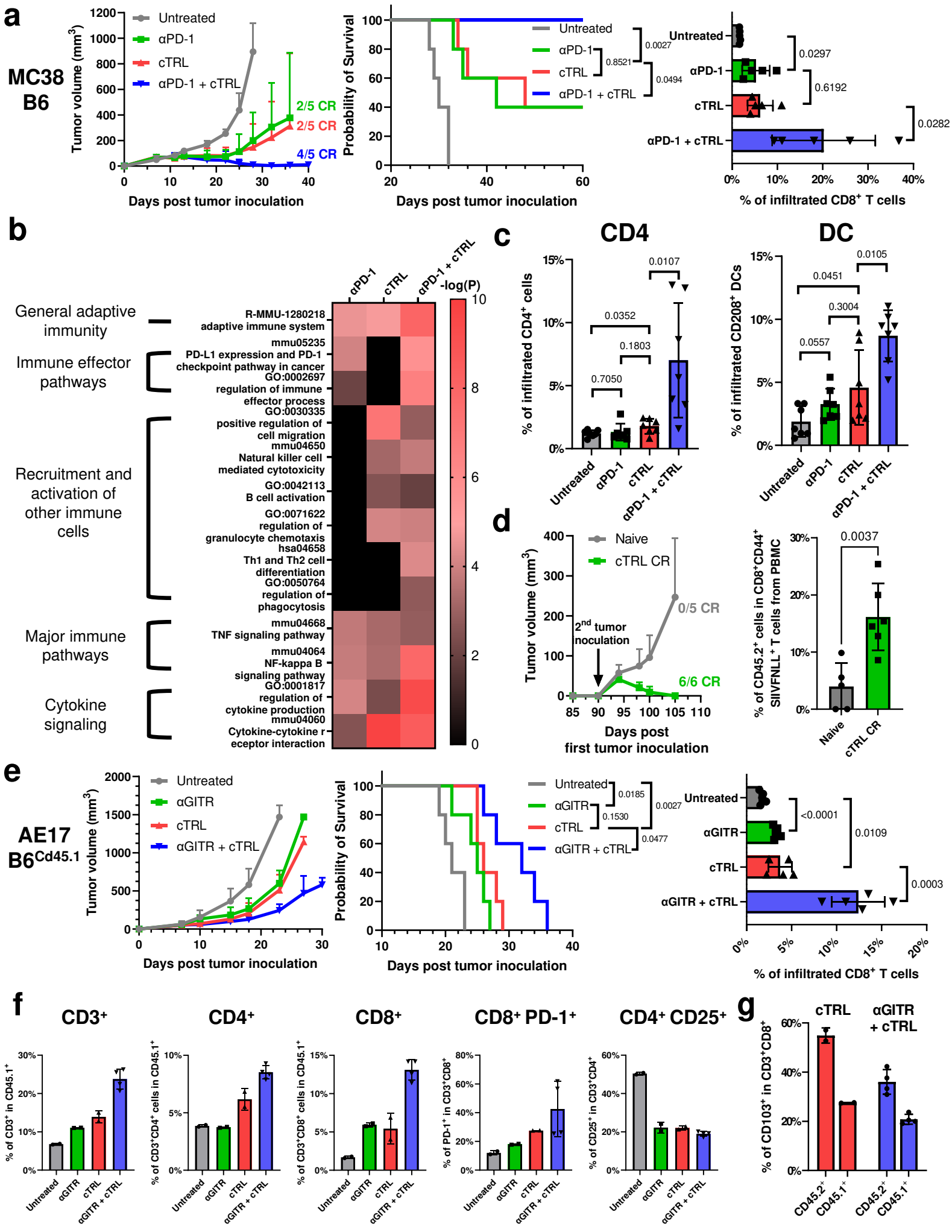
a
MC38
B6
Tumor volume (mm3)
Untreated
αPD-1
cTRL
αPD-1 + cTRL
2/5 CR
2/5 CR
4/5 CR
Days post tumor inoculation
Probability of Survival
0.0027
0.8521
0.0494
% of infiltrated CD8+ T cells
0.0297
0.6192
0.0282
b
General adaptive immunity
Immune effector pathways
Recruitment and activation of other immune cells
Major immune pathways
Cytokine signaling
-log(P)
R-MMU-1280218 adaptive immune system
mmu05235 PD-L1 expression and PD-1 checkpoint pathway in cancer
GO:0002697 regulation of immune effector process
GO:0030335 positive regulation of cell migration
mmu04650 Natural killer cell mediated cytotoxicity
GO:0042113 B cell activation
GO:0071622 regulation of granulocyte chemotaxis
hsa04658 Th1 and Th2 cell differentiation
GO:0050764 regulation of phagocytosis
mmu04668 TNF signaling pathway
mmu04064 NF-kappa B signaling pathway
GO:0001817 regulation of cytokine production
mmu04060 Cytokine-cytokine receptor interaction
c
CD4
% of infiltrated CD4+ cells
0.0107
0.0352
0.1803
0.7050
DC
% of infiltrated CD208+ DCs
0.0105
0.0451
0.3004
0.0557
d
Naive
cTRL CR
Tumor volume (mm3)
2nd tumor noculation
0/5 CR
6/6 CR
Days post first tumor inoculation
% of CD45.2+ cells in CD8+CD44+ SIIVFNLL+ T cells from PBMC
0.0037
e
AE17
B6Cd45.1
αGITR
αGITR + cTRL
<0.0001
0.0109
0.0003
f
CD3+
CD4+
CD8+
CD8+ PD-1+
CD4+ CD25+
g
cTRL
αGITR + cTRL
% of CD103+ in CD3+CD8+
CD45.2+ CD45.1+

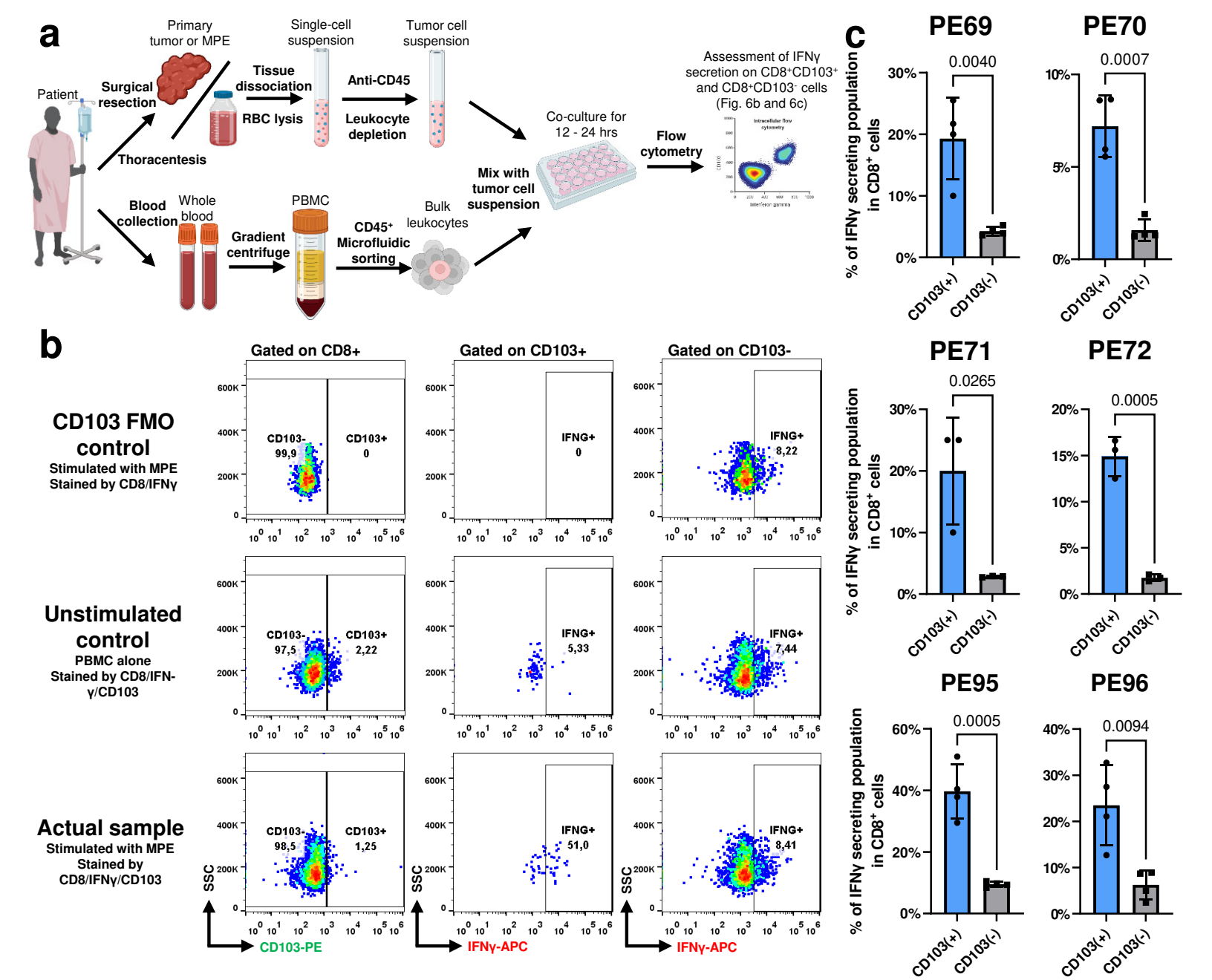
a
Patient
Surgical resection
Primary tumor or MPE
Thoracentesis
Tissue dissociation
RBC lysis
Single-cell suspension
Anti-CD45
Leukocyte depletion
Tumor cell suspension
Co-culture for 12 - 24 hrs
Mix with tumor cell suspension
Flow cytometry
Assessment of IFNγ secretion on CD8+CD103+ and CD8+CD103- cells (Fig. 6b and 6c)
Blood collection
Whole blood
Gradient centrifuge
PBMC
CD45+ Microfluidic sorting
Bulk leukocytes
b
Gated on CD8+
Gated on CD103+
Gated on CD103-
CD103 FMO control
Stimulated with MPE
Stained by CD8/IFNγ
CD103- 99,9
CD103+ 0
IFNG+ 0
IFNG+ 8,22
Unstimulated control
PBMC alone
Stained by CD8/IFN-γ/CD103
CD103- 97,5
CD103+ 2,22
IFNG+ 5,33
IFNG+ 7,44
Actual sample
Stimulated with MPE
Stained by CD8/IFNγ/CD103
CD103- 98,5
CD103+ 1,25
IFNG+ 51,0
IFNG+ 8,41
SSC
CD103-PE
IFNγ-APC
IFNγ-APC
c
PE69
PE70
PE71
PE72
PE95
PE96
0.0040
0.0007
0.0265
0.0005
0.0005
0.0094
% of IFNγ secreting population in CD8+ cells
CD103(+)
CD103(-)

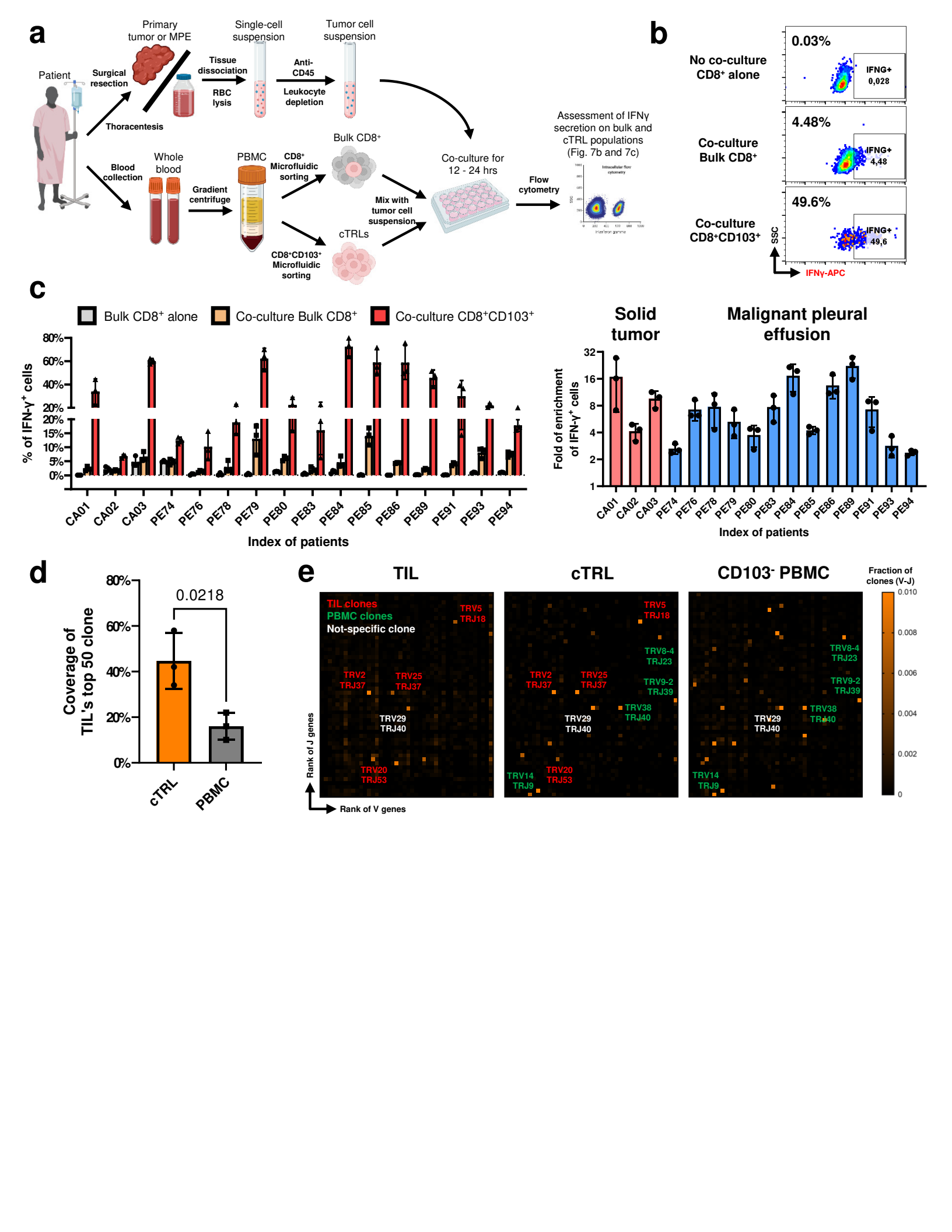
a
Patient
Surgical resection
Primary tumor or MPE
Thoracentesis
Tissue dissociation
RBC lysis
Single-cell suspension
Anti-CD45
Leukocyte depletion
Tumor cell suspension
Blood collection
Whole blood
Gradient centrifuge
PBMC
CD8+ Microfluidic sorting
Bulk CD8+
CD8+CD103+ Microfluidic sorting
cTRLs
Mix with tumor cell suspension
Co-culture for 12 - 24 hrs
Flow cytometry
Assessment of IFNγ secretion on bulk and cTRL populations (Fig. 7b and 7c)
b
No co-culture CD8+ alone
0.03%
IFNG+ 0,028
Co-culture Bulk CD8+
4.48%
IFNG+ 4,48
Co-culture CD8+CD103+
49.6%
IFNG+ 49,6
SSC
IFNγ-APC
c
Bulk CD8+ alone
Co-culture Bulk CD8+
Co-culture CD8+CD103+
% of IFN-γ+ cells
Index of patients
Solid tumor
Malignant pleural effusion
Fold of enrichment of IFN-γ+ cells
CA01 CA02 CA03 PE74 PE76 PE78 PE79 PE80 PE83 PE84 PE85 PE86 PE89 PE91 PE93 PE94
d
Coverage of TIL's top 50 clone
0.0218
cTRL
PBMC
e
TIL
cTRL
CD103- PBMC
Fraction of clones (V-J)
TIL clones
PBMC clones
Not-specific clone
TRV5 TRJ18
TRV2 TRJ37
TRV25 TRJ37
TRV29 TRJ40
TRV20 TRJ53
TRV8-4 TRJ23
TRV9-2 TRJ39
TRV38 TRJ40
TRV14 TRJ9
Rank of J genes
Rank of V genes

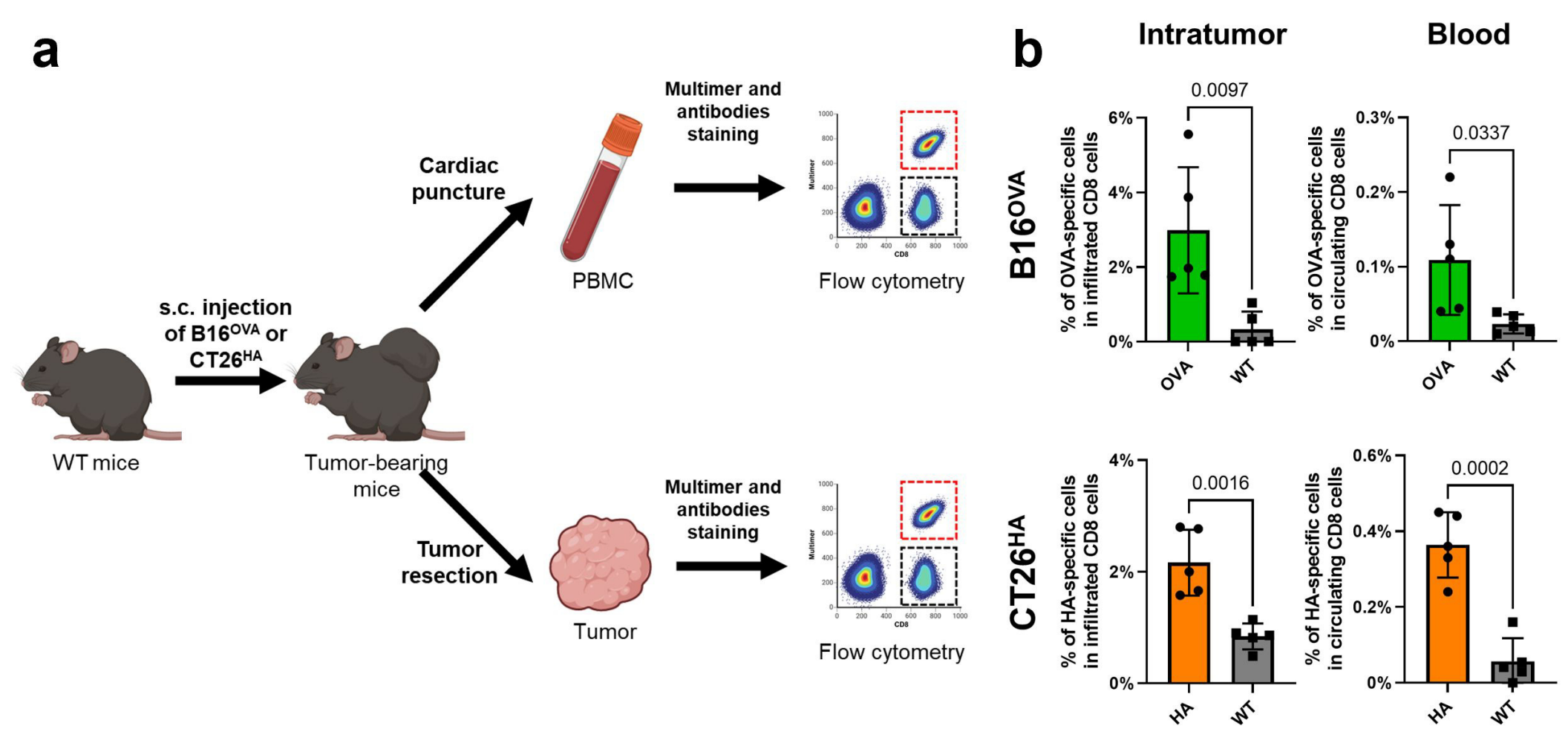
a
WT mice
s.c. injection of B16OVA or CT26HA
Tumor-bearing mice
Cardiac puncture
PBMC
Tumor resection
Tumor
Multimer and antibodies staining
Multimer and antibodies staining
Flow cytometry
Flow cytometry
b
Intratumor
Blood
B16OVA
% of OVA-specific cells in infiltrated CD8 cells
0.0097
OVA
WT
% of OVA-specific cells in circulating CD8 cells
0.0337
OVA
WT
CT26HA
% of HA-specific cells in infiltrated CD8 cells
0.0016
HA
WT
% of HA-specific cells in circulating CD8 cells
0.0002
HA
WT

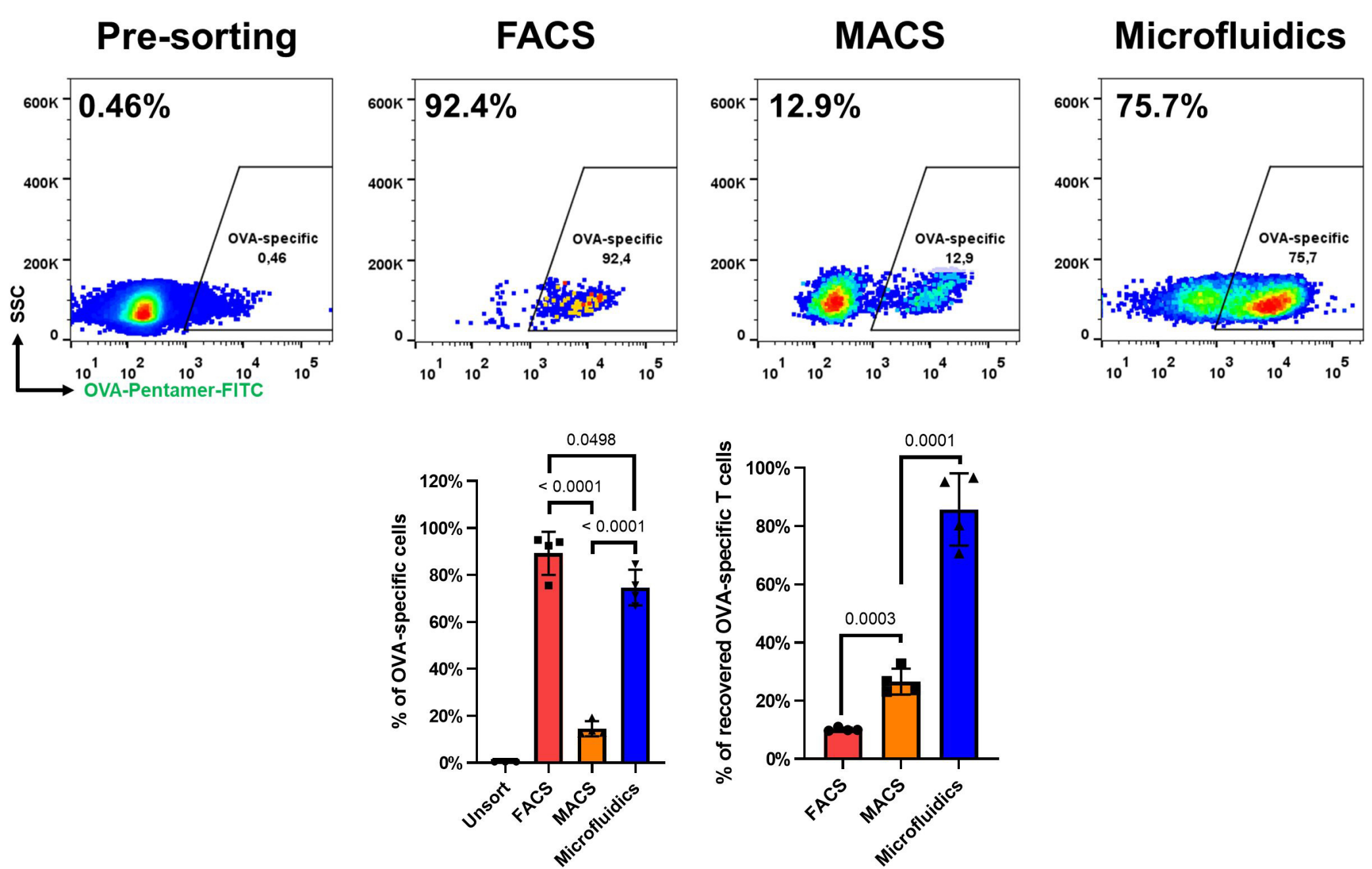
Pre-sorting
FACS
MACS
Microfluidics
0.46%
92.4%
12.9%
75.7%
OVA-specific
0,46
OVA-specific
92,4
OVA-specific
12,9
OVA-specific
75,7
600K
400K
200K
0
SSC
OVA-Pentamer-FITC
0.0498
< 0.0001
< 0.0001
% of OVA-specific cells
120%
100%
80%
60%
40%
20%
0%
Unsort
FACS
MACS
Microfluidics
0.0001
0.0003
% of recovered OVA-specific T cells

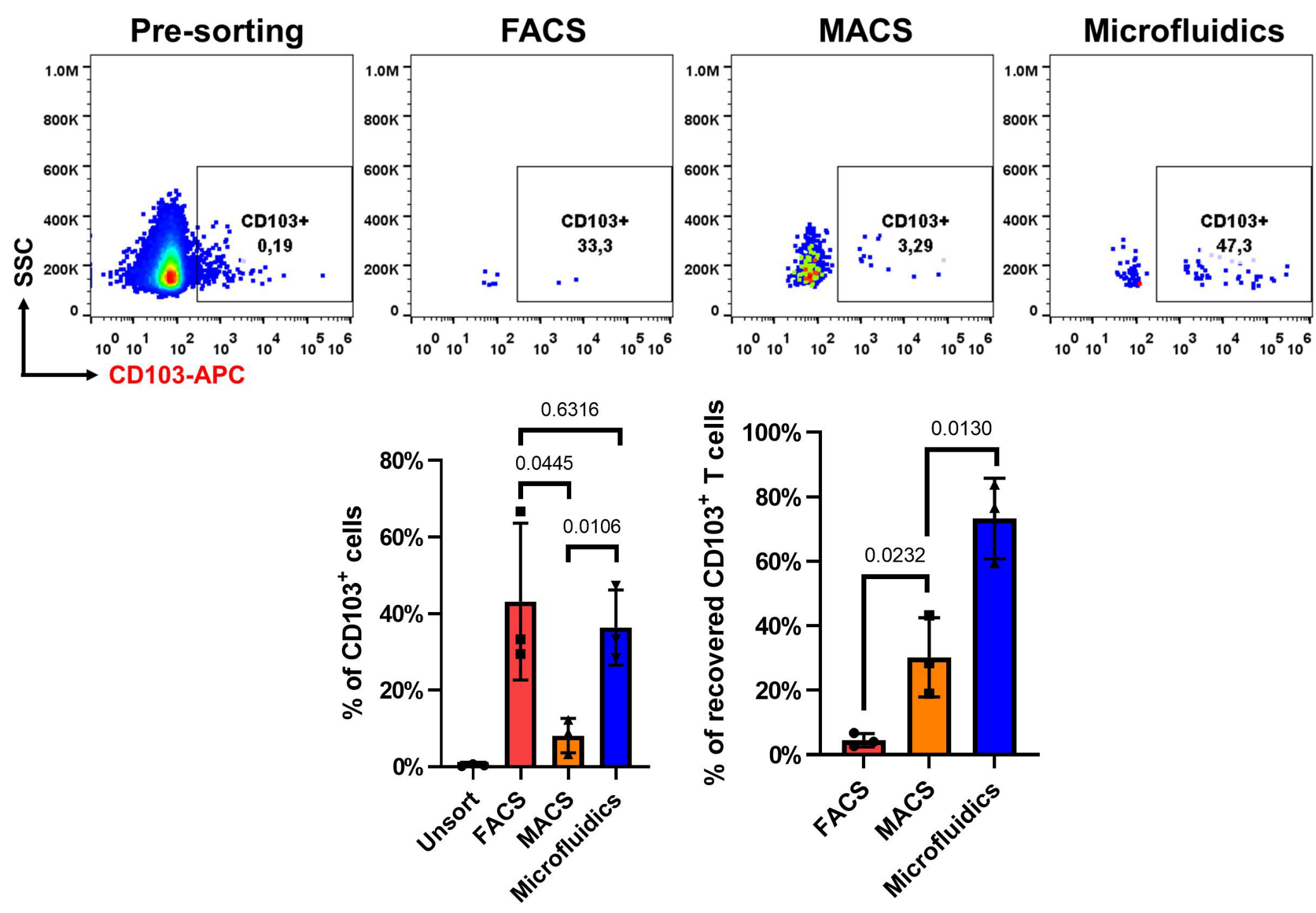
Pre-sorting
FACS
MACS
Microfluidics
SSC
CD103-APC
CD103+
0,19
CD103+
33,3
CD103+
3,29
CD103+
47,3
% of CD103+ cells
0.6316
0.0445
0.0106
Unsort
FACS
MACS
Microfluidics
% of recovered CD103+ T cells
0.0130
0.0232
FACS
MACS
Microfluidics

LLC-1
B6

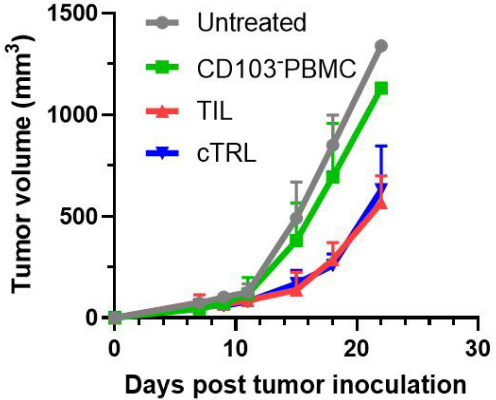
Untreated
CD103⁻PBMC
TIL
cTRL
Tumor volume (mm³)
1500
1000
500
0
0
10
20
30
Days post tumor inoculation

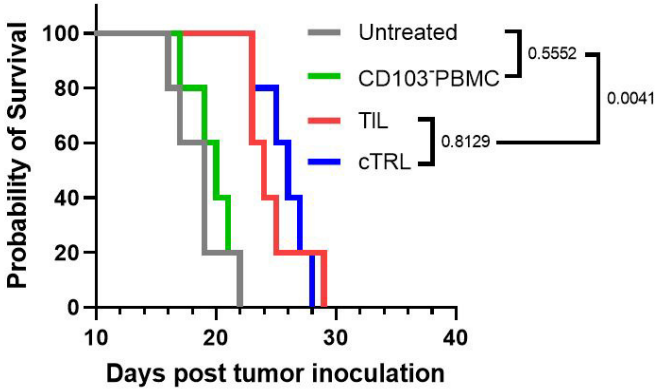
Untreated
CD103⁻PBMC
TIL
cTRL
0.5552
0.8129
0.0041
Probability of Survival
100
80
60
40
20
0
10
20
30
40
Days post tumor inoculation

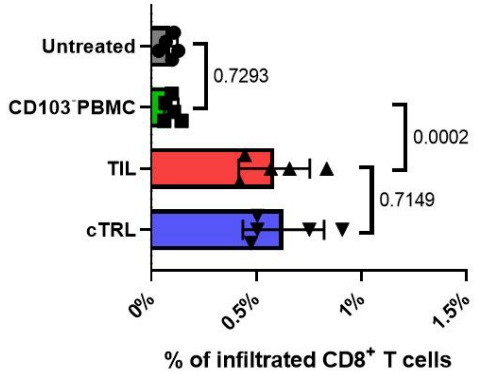
Untreated
CD103⁻PBMC
TIL
cTRL
0.7293
0.0002
0.7149
0%
0.5%
1%
1.5%
% of infiltrated CD8⁺ T cells

Untreated

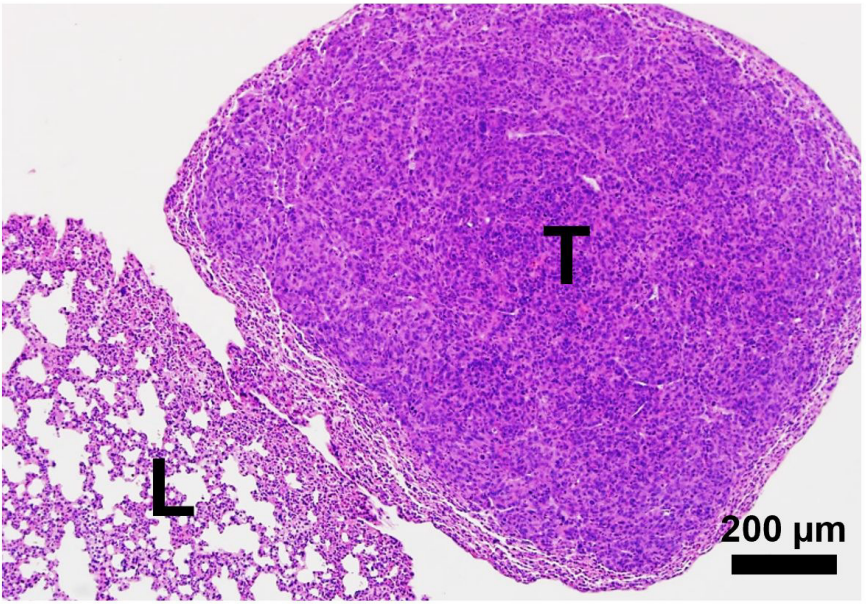

CD103⁻ PBMC

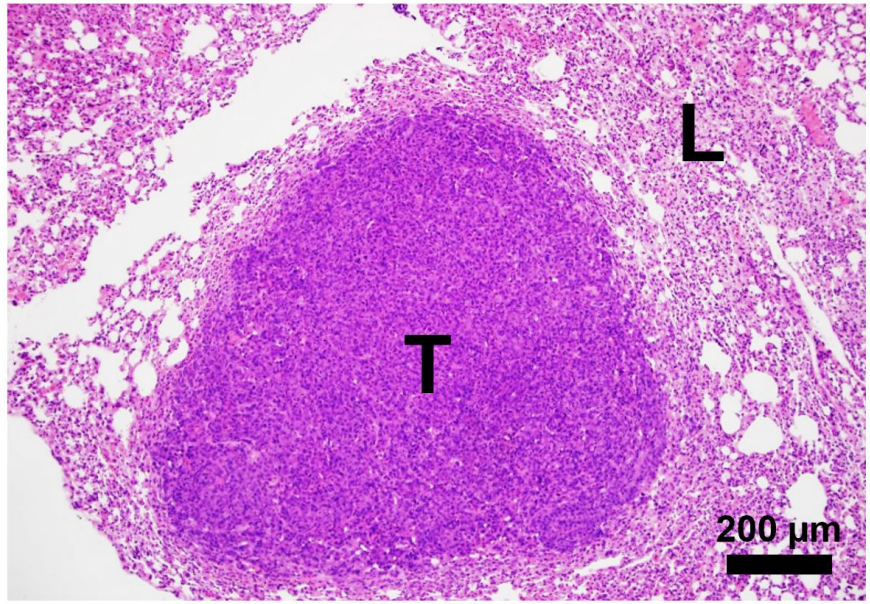

cTRL

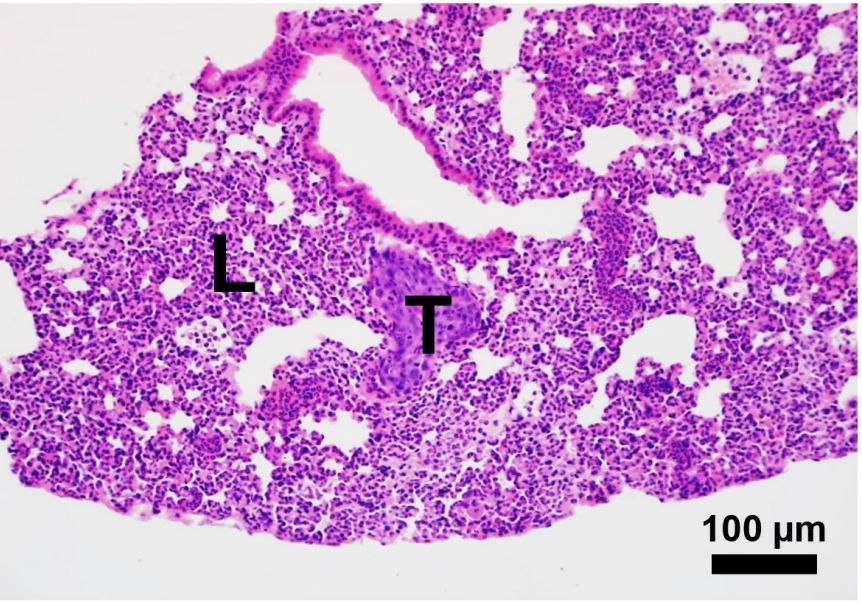

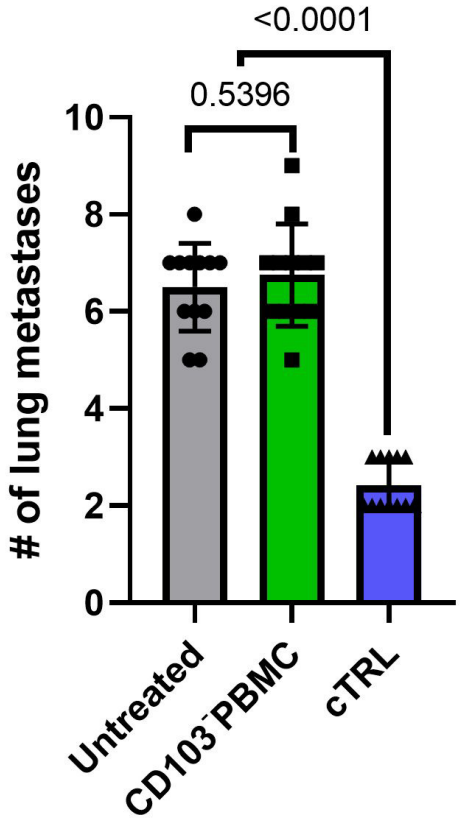

MC38
B6$^{Rag1-/-}$

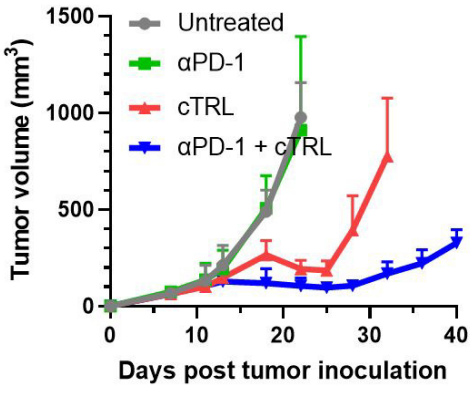
Tumor volume (mm^3)
1500
1000
500
0
Untreated
αPD-1
cTRL
αPD-1 + cTRL
0
10
20
30
40
Days post tumor inoculation

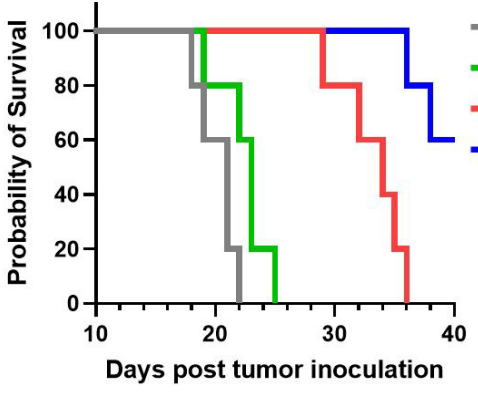
Probability of Survival
100
80
60
40
20
0
10
20
30
40
Days post tumor inoculation

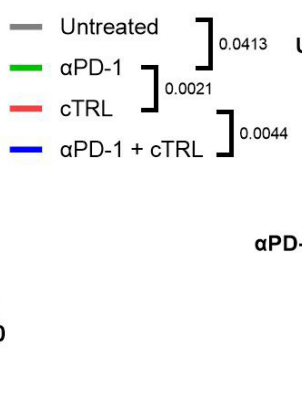
Untreated
αPD-1
cTRL
αPD-1 + cTRL
0.0413
0.0021
0.0044

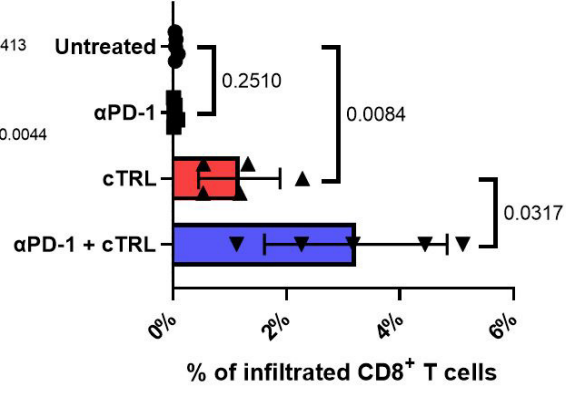
Untreated
αPD-1
cTRL
αPD-1 + cTRL
0.2510
0.0084
0.0317
0%
2%
4%
6%
% of infiltrated CD8$^+$ T cells